Arends, M., and Bradley, A. (2011) Mutant nucleophosmin and cooperating pathways drive leukemia initiation and progression in mice. *Nat. Genet.* **43,** 470–475

35. den Besten, W., Kuo, M. L., Williams, R. T., and Sherr, C. J. (2005) Myeloid leukemia-associated nucleophosmin mutants perturb p53-dependent and independent activities of the Arf tumor suppressor protein. *Cell Cycle* **4,** 1593–1598
36. Bhat, U. G., Jagadeeswaran, R., Halasi, M., and Gartel, A. L. (2011) Nucleophosmin interacts with FOXM1 and modulates the level and localization of FOXM1 in human cancer cells. *J. Biol. Chem.* **286,** 41425–41433
37. Taura, M., Suico, M. A., Fukuda, R., Koga, T., Shuto, T., Sato, T., Morino-Koga, S., Okada, S., and Kai, H. (2011) MEF/ELF4 transactivation by E2F1 is inhibited by p53. *Nucleic Acids Res.* **39,** 76–88

Transforming mutations of RAC guanosine triphosphatases in human cancers

Masahito Kawazu[a], Toshihide Ueno[b], Kenji Kontani[c], Yoshitaka Ogita[c], Mizuo Ando[a], Kazutaka Fukumura[a], Azusa Yamato[b], Manabu Soda[b], Kengo Takeuchi[d], Yoshio Miki[e], Hiroyuki Yamaguchi[a], Takahiko Yasuda[a,f], Tomoki Naoe[f], Yoshihiro Yamashita[b], Toshiaki Katada[c], Young Lim Choi[a], and Hiroyuki Mano[a,b,g,1]

[a]Department of Medical Genomics, Graduate School of Medicine, University of Tokyo, Tokyo 113-0033, Japan; [b]Division of Functional Genomics, Jichi Medical University, Tochigi 329-0498, Japan; [c]Department of Physiological Chemistry, Graduate School of Pharmaceutical Sciences, University of Tokyo, Tokyo 113-0033, Japan; [d]Pathology Project for Molecular Targets, The Cancer Institute, Japanese Foundation for Cancer Research, Tokyo 135-8550, Japan; [e]Department of Genetic Diagnosis, The Cancer Institute, Japanese Foundation for Cancer Research, Tokyo 135-8550, Japan; [f]Department of Hematology and Oncology, Nagoya University Graduate School of Medicine, Nagoya 466-8550, Japan; and [g]Core Research for Evolutional Science and Technology, Japan Science and Technology Agency, Saitama 332-0012, Japan

Edited by Shuh Narumiya, Kyoto University Faculty of Medicine, Kyoto, Japan, and accepted by the Editorial Board January 9, 2013 (received for review September 22, 2012)

Members of the RAS superfamily of small guanosine triphosphatases (GTPases) transition between GDP-bound, inactive and GTP-bound, active states and thereby function as binary switches in the regulation of various cellular activities. Whereas HRAS, NRAS, and KRAS frequently acquire transforming missense mutations in human cancer, little is known of the oncogenic roles of other small GTPases, including Ras-related C3 botulinum toxin substrate (RAC) proteins. We show that the human sarcoma cell line HT1080 harbors both NRAS(Q61K) and RAC1(N92I) mutant proteins. Whereas both of these mutants were able to transform fibroblasts, knockdown experiments indicated that RAC1(N92I) may be the essential growth driver for this cell line. Screening for RAC1, RAC2, or RAC3 mutations in cell lines and public databases identified several missense mutations for RAC1 and RAC2, with some of the mutant proteins, including RAC1(P29S), RAC1(C157Y), RAC2(P29L), and RAC2(P29Q), being found to be activated and transforming. P29S, N92I, and C157Y mutants of RAC1 were shown to exist preferentially in the GTP-bound state as a result of a rapid transition from the GDP-bound state, rather than as a result of a reduced intrinsic GTPase activity. Activating mutations of RAC GTPases were thus found in a wide variety of human cancers at a low frequency; however, given their marked transforming ability, the mutant proteins are potential targets for the development of new therapeutic agents.

oncogene | resequencing

The identification of transforming proteins and the development of agents that target them have markedly influenced the treatment and improved the prognosis of individuals with cancer. Chronic myeloid leukemia (CML), for example, has been shown to result from the growth-promoting activity of the fusion tyrosine kinase breakpoint cluster region-Abelson murine leukemia viral oncogene homolog 1 (BCR-ABL1), and treatment with a specific ABL1 inhibitor, imatinib mesylate, has increased the 5-y survival rate of individuals with CML to almost 90% (1). Similarly, the fusion of echinoderm microtubule associated protein like 4 gene (*EML4*) to anaplastic lymphoma receptor tyrosine kinase (*ALK*) is responsible for a subset of non–small-cell lung cancer cases (2), and therapy targeted to EML4-ALK kinase activity has greatly improved the progression-free survival of affected individuals compared with that achieved with conventional chemotherapies (3). Therapies that target essential growth drivers in human cancers are thus among the most effective treatments for these intractable disorders.

V-Ki-ras2 Kirsten rat sarcoma viral oncogene homolog (KRAS), v-Ha-ras Harvey rat sarcoma viral oncogene homolog (HRAS), and neuroblastoma RAS viral (v-ras) oncogene homolog (NRAS) are the founding members of the rat sarcoma (RAS) superfamily of small guanosine triphosphatases (GTPases) that is known to comprise >150 members in humans (4). Five subgroups of these small GTPases have been identified and designated as the RAS; ras homolog family member (RHO); RAB1A, member RAS oncogene family (RAB); RAN, member RAS oncogene family (RAN); and ADP-ribosylation factor (ARF) families. All small GTPases function as binary switches that transition between GDP-bound, inactive and GTP-bound, active forms and thereby contribute to intracellular signaling that underlies a wide array of cellular activities, including cell proliferation, differentiation, survival, motility, and transformation (5). Somatic point mutations that activate KRAS, HRAS, or NRAS have been identified in a variety of human tumors, with KRAS being the most frequently activated oncoprotein in humans. Somatic activating mutations of KRAS are thus present in >90% of pancreatic adenocarcinomas, for example (6). Surprisingly, however, mutational activation of small GTPases other than KRAS, HRAS, and NRAS has not been widely reported.

Ras-related C3 botulinum toxin substrate (RAC) 1, RAC2, and RAC3 belong to the RHO family of small GTPases (7). RAC proteins orchestrate actin polymerization, and their activation induces the formation of membrane ruffles and lamellipodia (8), which play essential roles in the maintenance of cell morphology and in cell migration. Accumulating evidence also indicates that RAC proteins function as key hubs of intracellular signaling that underlies cell transformation. RAC1, for example, serves as an essential downstream component of the signaling pathway by which oncogenic RAS induces cell transformation, and artificial introduction of an amino acid substitution (G12V) into RAC1 renders it oncogenic (9). Furthermore, suppression of RAC1 activity induces apoptosis in glioma cells (10), and loss of *RAC1* or *RAC2* results in a marked delay in the development of BCR-ABL1–driven myeloproliferative disorder (11). Despite such important roles of RAC proteins in cancer, somatic transforming mutations of these proteins have not been identified in cancer specimens.

We have now discovered a mutant form of RAC1 with the amino acid substitution N92I in a human sarcoma cell line, HT1080, and have found that this mutation renders RAC1 constitutively active and highly oncogenic. Even though HT1080 cells also harbor the NRAS(Q61K) oncoprotein, RAC1(N92I) is the essential growth driver in this cell line, given that RNA interference (RNAi)-

Author contributions: M.K. and H.M. designed research; M.K., T.U., K.K., Y.O., M.A., K.F., A.Y., M.S., K.T., Y.M., H.Y., T.Y., T.N., Y.Y., T.K., and Y.L.C. performed research; M.K., T.U., K.K., Y.O., K.T., T.N., T.K., Y.L.C., and H.M. analyzed data; and H.M. wrote the paper.

The authors declare no conflict of interest.

This article is a PNAS Direct Submission. S.N. is a guest editor invited by the Editorial Board.

[1]To whom correspondence should be addressed. E-mail: hmano@m.u-tokyo.ac.jp.

This article contains supporting information online at www.pnas.org/lookup/suppl/doi:10.1073/pnas.1216141110/-/DCSupplemental.

mediated knockdown of RAC1(N92I) markedly suppressed cell growth. Further screening for *RAC1*, *RAC2*, and *RAC3* mutations among cancer cell lines as well as public databases identified additional transforming mutations of RAC1 and RAC2. Our data thus reveal oncogenic amino acid substitutions for the RAC subfamily of small GTPases in human cancer.

Results

Discovery of the RAC1(N92I) Oncoprotein. To identify transforming genes in the fibrosarcoma cell line HT1080 (12), we isolated cDNAs for cancer-related genes (n = 906) from HT1080 cells and subjected them to deep sequencing with the Genome Analyzer IIx (GAIIx) system. Quality filtering of the 92,025,739 reads obtained yielded 45,325,377 unique reads that mapped to 843 (93.0%) of the 906 target genes. The mean read coverage for the 843 genes was 495× per nucleotide, and ≥70% of the captured regions for 568 genes were read at ≥10× coverage.

Screening for nonsynonymous mutations in the data set with the use of our computational pipeline (13) revealed a total of five missense mutations with a threshold of ≥30× coverage and a ≥30% mutation ratio (Table S1). One of these mutations, a heterozygous missense mutation of *NRAS* that results in a Gln-to-Lys substitution at amino acid position 61 (Q61K), was described previously in this cell line (14) and is the most frequent transforming mutation of *NRAS* (5). We also discovered a missense mutation in another small GTPase, RAC1 (Fig. S1 and Table S1). An A-to-T transversion at position 516 of human *RAC1* cDNA (GenBank accession no. NM_006908.4), resulting in an Asn-to-Ile substitution at position 92 of the encoded protein, was thus identified in 11,525 (47.5%) of the 24,238 total reads covering this position.

To examine the transforming potential of RAC1(N92I), we infected mouse 3T3 fibroblasts and MCF10A human mammary epithelial cells (15) with a retrovirus encoding wild-type or N92I mutant form of human RAC1 and then seeded the cells in soft agar for evaluation of anchorage-independent growth. Neither 3T3 nor MCF10A cells expressing wild-type RAC1 grew in soft agar (Fig. 1*A*), indicating the lack of transforming potential of RAC1. In contrast, the cells expressing RAC1(N92I) readily grew in soft agar (Fig. 1*A*), showing that this RAC1 mutant confers the property of anchorage-independent growth on both 3T3 and MCF10A cells. We also confirmed the transforming potential of an artificial mutant of RAC1, RAC1(G12V) (8),

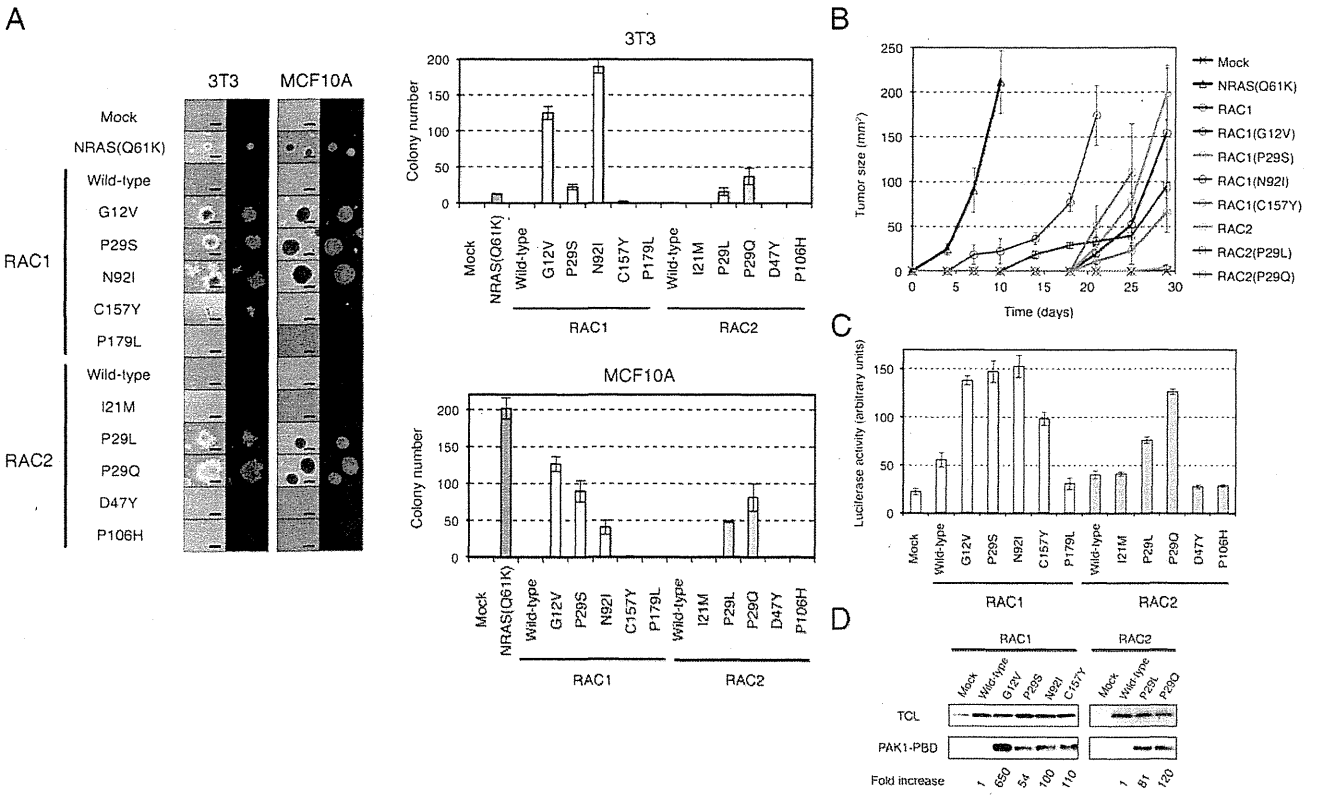

Fig. 1. Transforming potential of RAC1 and RAC2 mutants. (*A*) 3T3 or MCF10A cells were infected with recombinant retroviruses encoding enhanced green fluorescent protein (EGFP) as well as wild-type or mutant forms of RAC1 or RAC2 and were then assayed for anchorage-independent growth in vitro under the presence of 10% (vol/vol) FBS. After 14 d (3T3) or 20 d (MCF10A) of culture, the cells were stained with crystal violet and examined by conventional microscopy (*Left*: left image of each pair), and they were monitored for EGFP expression by fluorescence microscopy (*Left*: right image of each pair). (Scale bars, 0.5 mm.) The numbers of cell colonies were also determined as means ± SD from three independent experiments (*Right*). (*B*) 3T3 cells expressing wild-type or mutant forms of RAC1 or RAC2 were injected s.c. into the shoulder of nude mice, and the size of the resulting tumors [(length × width)/2] was determined at the indicated times thereafter. Tumor size for 3T3 expressing NRAS(Q61K) was similarly monitored. Data are means ± SD for tumors at four injection sites. (*C*) HEK293T cells were transfected with expression vectors for wild-type or mutant forms of RAC1 or RAC2 together with the SRE.L reporter plasmid and pGL-TK. The activity of firefly luciferase in cell lysates was then measured and normalized by that of *Renilla* luciferase. Data are means ± SD from three independent experiments. (*D*) Lysates of 3T3 cells expressing wild-type or mutant forms of RAC1 or RAC2 were subjected to a pull-down assay with PAK1-PBD. The precipitated proteins as well as the total cell lysates were then subjected to immunoblot analysis with antibodies to RAC1 or to RAC2. The relative amounts of pulled-down RAC proteins compared with their corresponding expression levels in total cell lysate were normalized to that of wild-type RAC1 (for the RAC1 mutants) or RAC2 (for the RAC2 mutants) and are shown at the bottom.

which harbors an amino acid substitution corresponding to that of the oncogenic G12V mutant form of RAS proteins.

Other Transforming Mutations of RAC1 and RAC2. We next searched for other transforming mutations of RAC proteins. Human RAC1, RAC2 (GenBank accession no. NM_002872.3), and RAC3 (GenBank accession no. NM_005052.2) cDNAs were isolated from 40 cancer cell lines (Table S2), and their nucleotide sequences were determined by Sanger sequencing, resulting in the discovery of RAC1(P29S), RAC2(P29Q), and RAC2(P29L) in the breast cancer cell line MDA-MB-157, the CML cell line KCL-22, and the breast cancer cell line HCC1143, respectively (Fig. S1 and Table S3). Further searching for *RAC1*, *RAC2*, and *RAC3* mutations in the COSMIC database of cancer genome mutations (Release V59; http://cancer.sanger.ac.uk/cancergenome/projects/cosmic) revealed various amino acid substitutions detected in human tumors, namely RAC1(P29S), RAC1(C157Y), RAC1(P179L), RAC2(I21M), RAC2(P29L), RAC2(D47Y), and RAC2(P106H) (Table S3). Importantly, all of these *RAC1* and *RAC2* mutations identified in clinical specimens were confirmed to be somatic, given that the corresponding mutations were absent in the genome of paired normal cells.

To examine the transforming potential of these various RAC1 and RAC2 mutants, we expressed each protein in 3T3 and MCF10A cells and evaluated anchorage-independent growth. Whereas the wild-type form of RAC2 did not transform 3T3 or MCF10A cells, growth in soft agar was apparent for 3T3 cells expressing RAC1 (P29S), RAC1(C157Y), RAC2(P29L), or RAC2(P29Q), but not for those expressing RAC1(P179L), RAC2(I21M), RAC2(D47Y), or RAC2(P106H) (Fig. 1*A*). Of interest, colony number in the assay varied substantially in a manner dependent on the type of amino acid substitution as well as on cell type. RAC1(C157Y), for example, yielded fewer colonies in soft agar compared with the other transforming mutants. Furthermore, RAC1(P29S), which was identified in a breast cancer cell line, generated a larger number of colonies with MCF10A cells than with 3T3 cells. Conversely, RAC1(N92I), which was identified in a fibrosarcoma cell line, yielded a larger number of colonies with 3T3 cells than with MCF10A cells. The oncogenic activity of RAC1(P29S), RAC1 (N92I), RAC1(C157Y), RAC2(P29L), and RAC2(P29Q) mutants was further confirmed with a tumorigenicity assay in nude mice (Fig. 1*B*), with the activity of RAC1(N92I) being the most pronounced with regard to the transformation of 3T3 cells in this assay.

The colony number in soft agar for 3T3 cells expressing NRAS (Q61K) was fewer than that for the cells expressing oncogenic RAC1 or RAC2 mutants (Fig. 1*A*), whereas expression of these small GTPases was readily confirmed in 3T3 (Fig. S2). Interestingly, s.c. tumors from the same 3T3 cells expressing NRAS(Q61K) grew more rapidly than tumors expressing the RAC1/RAC2 mutants (Fig. 1*B*), indicating that the measured intensity of the transforming potential of GTPases may vary in a dependent manner on assay systems.

To examine whether such oncogenic potential is linked directly to the activation of RAC1 or RAC2, we investigated the activity of the mutant proteins with the use of a luciferase reporter plasmid that selectively responds to intracellular signaling evoked by RHO family GTPases (16). In concordance with the data from the soft agar and tumorigenicity assays, only the transforming mutants of RAC1 and RAC2 yielded a substantial level of luciferase activity in transfected HEK293T cells (Fig. 1*C*).

Activated RAC1 or RAC2 would be expected to be loaded with GTP. We therefore examined the GTP-binding status of the RAC1 and RAC2 oncoproteins with the use of a pull-down assay based on the p21-binding domain (PBD) of PAK1. All of the transforming RAC1 and RAC2 mutants were found to exist preferentially in the GTP-bound state (Fig. 1*D*), indicative of their constitutive activation. Furthermore, these RAC1 and RAC2 mutants induced marked reorganization of the actin cytoskeleton in 3T3 cells, resulting in the accumulation of polymerized actin in ruffles at the plasma membrane (Fig. 2).

RAC1 and RAC2 as Therapeutic Targets. Given that NRAS(Q61K) is also known to transform 3T3 cells (17) (Fig. 1*A*), our data show that HT1080 cells harbor two independent oncogenic GTPases. We therefore examined whether RAC1(N92I) or NRAS(Q61K) is the principal growth driver in this sarcoma cell line. Among several small interfering RNAs (siRNAs) designed to attenuate the expression of RAC1 or NRAS, we selected two independent siRNAs that specifically target each mRNA (Fig. 3*A*). Whereas transfection of HT1080 cells with either NRAS siRNA resulted in a moderate inhibition of cell proliferation under the presence of 10% (vol/vol) FBS, that with either RAC1 siRNA almost blocked cell growth (Fig. 3*B*). Transfection with an NRAS siRNA in addition to either RAC1 siRNA did not result in an additional effect on cell proliferation (Fig. 3*B*). Similar data were observed in a culture with 1% (vol/vol) FBS (Fig. S3*A*) or under FBS-free conditions (Fig. S3*B*). To further examine the effects of silencing RAC1/NRAS, we quantitated cell cycle distribution of HT1080 transfected with siRNAs against either RAC1 or NRAS. As shown in Fig. S4*A*, DNA synthesis was equally suppressed by the knockdown of RAC1 or NRAS. Interestingly, however, CASP3/CASP7 activity (a surrogate marker for apoptosis) was markedly induced only by RAC1 depletion (Fig. S4*B*). Therefore, RAC proteins are likely to provide RAS-independent cell survival

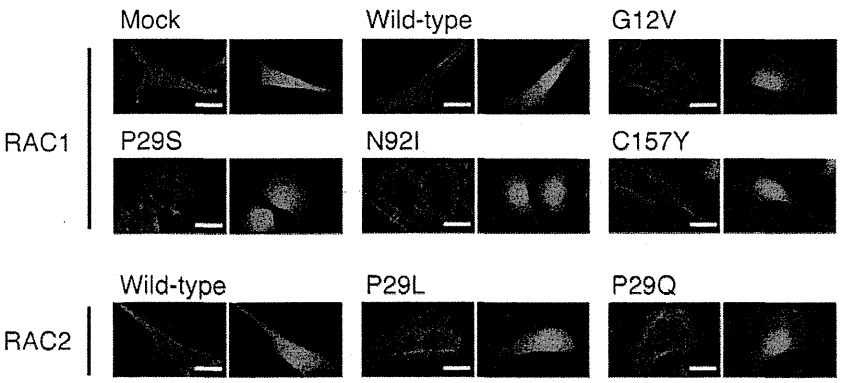

Fig. 2. Actin reorganization induced by the RAC1/RAC2 mutants. 3T3 cells infected with retroviruses encoding enhanced green fluorescent protein (EGFP) as well as wild-type or mutant forms of RAC1 or RAC2 were stained with Alexa Fluor 594-labeled phalloidin to visualize actin organization (*Left* image of each pair). The same cells were also examined for EGFP fluorescence (*Right* image of each pair). (Scale bars, 20 μm.)

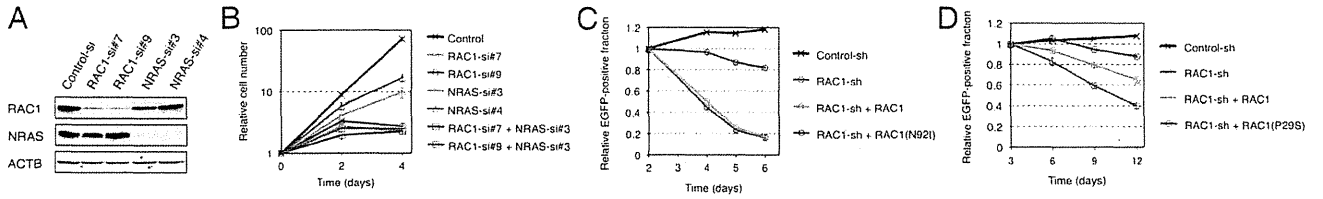

Fig. 3. Oncogenic RAC proteins as therapeutic targets. (*A*) HT1080 cells were transfected with control, RAC1, or NRAS siRNAs; lysed; and subjected to immunoblot analysis with antibodies to RAC1, NRAS, or ACTB (loading control). (*B*) HT1080 cells were transfected with control, RAC1, or NRAS siRNAs, as indicated, and cultured under the presence of 10% (vol/vol) FBS. Cell number was counted at the indicated times after the onset of transfection. Data are means ± SD from three independent experiments. (*C*) HT1080 cells were infected with a retrovirus encoding green fluorescent protein (EGFP) as well as a control or RAC1 shRNA. They were also infected with a retrovirus encoding shRNA-resistant wild-type RAC1 or RAC1(N92I), as indicated. The number of EGFP-positive cells was determined by flow cytometry after culture of the cells for the indicated times, and the size of the EGFP-positive fraction relative to that at 2 d was calculated. Data are means ± SD from three independent experiments. (*D*) MDA-MB-157 cells were infected with a retrovirus encoding EGFP as well as a control or RAC1 shRNA. They were also infected with a retrovirus encoding shRNA-resistant wild-type RAC1 or RAC1(P29S), as indicated. The number of EGFP-positive cells was determined by flow cytometry after culture of the cells for the indicated times, and the size of the EGFP-positive fraction relative to that at 3 d was calculated. Data are means ± SD from three independent experiments.

signals, which is supported by the fact that, even under FBS-free conditions, RAC1 depletion has more antiproliferative effects in HT1080 than NRAS depletion (Fig. S3*B*). These data show that active RAC1 may be the essential growth driver in HT1080 cells and is therefore a potential therapeutic target. Furthermore, our data suggest that oncogenic RAS proteins may require additional transforming hits to give rise to full-blown cancer.

We next infected HT1080 cells with a retrovirus expressing a short hairpin RNA (shRNA) targeted to RAC1 mRNA. Expression of the RAC1 shRNA markedly suppressed cell growth, whereas restoration of shRNA-resistant RAC1(N92I) expression reversed this effect (Fig. 3*C* and Fig. S5), showing that the effect of the RAC1 shRNA was not an off-target artifact. Forced expression of shRNA-resistant wild-type RAC1 failed to reverse the inhibitory effect of the RAC1 shRNA on cell growth, indicating that growth suppression by the shRNA was due to depletion of the N92I mutant, not to that of the wild-type protein. We performed similar experiments with the breast cancer cell line MDA-MB-157, which harbors RAC1(P29S). Again, the RAC1 shRNA inhibited cell growth, and this effect was reversed to a larger extent by restoration of the expression of shRNA-resistant RAC1(P29S) than by forced expression of the wild-type protein (Fig. 3*D* and Fig. S5).

RAC1(P29S), RAC1(N92I), and RAC1(C157Y) Are Rapid-Cycling Mutants. Oncogenic mutations at G12, G13, or Q61 of RAS proteins found in human tumors reduce the intrinsic GTPase activity of these

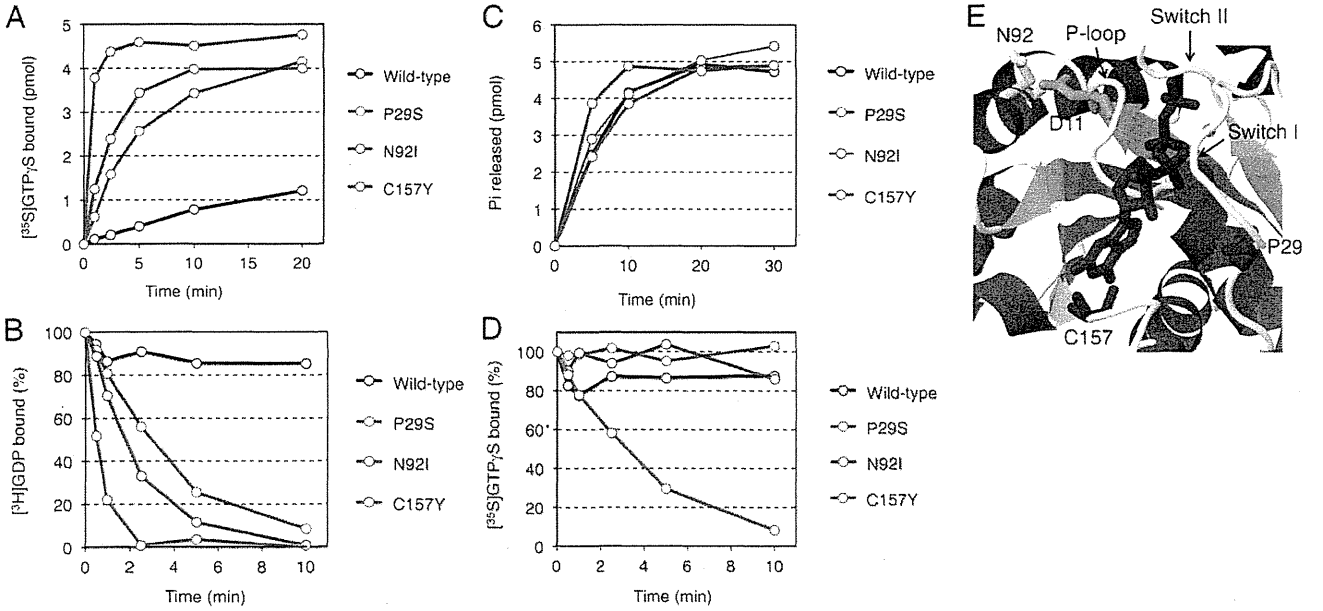

Fig. 4. Biochemical properties of RAC1 mutants. (*A*) Bacterially expressed and purified proteins of the wild-type, P29S, N92I, or C157Y mutant of RAC1 (5 pmol each) were incubated with [^{35}S]GTPγS in the presence of 0.8 mM Mg^{2+}, and the amounts of [^{35}S]GTPγS-bound proteins were determined at the indicated times. (*B*) [^{3}H]GDP dissociation from [^{3}H]GDP-bound RAC1 proteins was initiated by the addition of unlabeled GTPγS in the presence of 0.8 mM Mg^{2+}, and the amounts of [^{3}H]GDP-bound proteins were determined at the indicated times. (*C*) RAC1 proteins were preloaded with [γ^{32}P] GTP, and then GTP hydrolysis reactions were initiated by the addition of unlabeled GTP in the presence of 0.8 mM Mg^{2+}. P_i released from the proteins was isolated and measured at the indicated times. (*D*) [^{35}S]GTPγS dissociation from [^{35}S]GTPγS-bound RAC1 proteins was initiated by the addition of unlabeled GTPγS in the presence of 0.8 mM Mg^{2+}, and the amounts of [^{35}S]GTPγS-bound proteins were determined at the indicated times. (*E*) Schematic representation of the structure of the GTP-binding pocket of human RAC1 (ID 1mh1 in the Protein Data Bank; www.pdb.org) with α-helices and β-sheets shown in magenta and orange, respectively. The GTP analog guanosine 5′-(β,γ-imido)-triphosphate (GppNp) and Mg^{2+} are depicted in red and green, respectively. D11, P29, N92, and C157 amino acid residues are in orange, blue, yellow and purple, respectively. The positions of switch I and switch II regions and the P-loop are also indicated.

proteins and thereby maintain them in the GTP-bound state (18, 19). On the other hand, an artificial F28L substitution in HRAS or the RHO family protein Cdc42Hs was shown to confer constitutive activity by accelerating the transition from the GDP-bound to the GTP-bound state without the involvement of an exogenous guanine nucleotide exchange factor (GEF) (20, 21).

To determine how transforming mutations of RAC1 results in constitutive activation of these proteins, we examined their affinity for GTP and GDP. Compared with wild-type RAC1, all of RAC1(P29S), RAC1(N92I), and RAC1(C157Y) was found to bind GTPγS (nonhydrolyzable GTP analog) rapidly in vitro, even without the addition of a GEF protein (Fig. 4*A*). Likewise, the dissociation of GDP from the mutant forms of RAC1 was greatly accelerated (Fig. 4*B*). On the other hand, the intrinsic GTPase activity of these mutants was similar to (for P29S and N92I) or slightly higher (for C157Y) than that of the wild-type protein (Fig. 4*C*). These data thus indicated that, in contrast to transforming RAS mutants associated with human cancer, RAC1 (P29S), RAC1(N92I), and RAC1(C157Y) are fast-cycling mutants, for which the probability of being in the GTP-bound state is increased as the result of an increased rate of GDP dissociation, rather than as the result of a loss of GTPase activity.

Interestingly, dissociation of GTPγS was also accelerated only for RAC1(C157Y), but not for the wild-type, P29S, or N92I form of RAC1 (Fig. 4*D*). Thus, RAC1(C157Y) is a unique mutant in that both association and dissociation for GTP are accelerated, which may provide the molecular basis for its modest transforming potential compared with that of RAC1(P29S) or RAC1 (N92I) (Fig. 1).

In the 3D structure of RAC1 (Fig. 4*E*), P29 is located in the switch I region, whereas C157 is positioned adjacent to the guanine ring of bound GTP. Substitution of these residues would thus likely affect the affinity of the protein for GDP or GTP (Fig. S6), a phenomenon that has been demonstrated recently for RAC1 (P29S) (22). In contrast, N92 is located distant from the binding pocket for GDP/GTP, and so the structural mechanism by which the N92I substitution renders RAC1 constitutively active remains elusive (Fig. 4*E* and Fig. S6). Residue N92 is located close to D11 in the P-loop of RAC1, however (Fig. 4*E* and Fig. S7), and substitution with isoleucine at this position would abolish the interaction between the amino group of N92 and the carboxyl group of D11. It is thus possible that the N92I mutation affects the binding of GDP/GTP through an effect on the P-loop.

Discussion

We have here demonstrated the transforming potential of mutated RAC proteins. Our analysis of cell lines resulted in the identification of transforming mutants of RAC1 and RAC2, namely RAC1(N92I) and RAC2(P29Q), and we also revealed the transforming potential of the RAC1(P29S), RAC1(C157Y), and RAC2(P29L) mutants deposited the COSMIC database of cancer genome mutations (Release V59; http://cancer.sanger.ac.uk/cancergenome/projects/cosmic) (Table S3). In contrast, the soft agar assay did not reveal a transforming potential of the RAC1(P179L), RAC2(I21M), RAC2(D47Y), or RAC2(P106H) mutants found in the database, suggesting a possibility that they are "passenger mutations." It may also be possible, however, that these mutants may still contribute to cancer development by modifying tumor properties (such as metastasis ability), given that they were somatically acquired and clonally selected in cancer.

An important finding of our study was that the oncogenic effects of RAC1(N92I) may be more pronounced than those of NRAS(Q61K), at least with regard to survival signals in HT1080 cells (Fig. 3*B*). It should be noted, however, that HT1080 expresses RAC1 almost exclusively among the RAC family proteins, whereas HRAS and KRAS are weakly expressed in addition to NRAS (Fig. S8). It is thus possible that the effects of NRAS knockdown in Fig. 3*B* may be partly complemented by the residual HRAS/KRAS proteins.

Paterson et al. previously isolated NRAS-attenuated subclones of HT1080 after treatment with an alkylating reagent (*N*-methyl-*N'*-nitro-*N*-nitrosoguanidine) and a subsequent culture with 5-fluorodeoxyuridine and 1-β-D-arabinofuranosylcytosine (23). Such subclones had a flat cell shape and a reduced ability for anchorage-independent growth. Likewise, we noted that transfection with NRAS siRNAs renders HT1080 a flatter shape (Fig. S9). As demonstrated in Fig. 3*B* and by Paterson et al. (23), however, such NRAS-depleted HT1080 was still viable and kept proliferation in vitro, suggesting the presence of other oncogene(s) in addition to NRAS(Q61K). Therefore, NRAS(Q61K) and RAC1(N92I) are likely to cooperate to fully transform this fibrosarcoma.

Regarding the coexistence of mutations within RAC family proteins and RAS-RAF-MAPK proteins, two studies independently reported recurrent P29S mutation of RAC1 in melanoma during the preparation of this article (22, 24). Of note, BRAF (V600E) was also detected in four of six and in two of seven of the RAC mutation-positive melanomas, respectively. These observations, together with our findings with HT1080 cells, thus indicate that activating mutations of RAC1 and those of the RAS-RAF–signaling pathway are not mutually exclusive.

Members of the RAC subfamily of GTPases show a high level of sequence identity in humans. The amino acid sequence of RAC1 is thus 92% identical to that of RAC2 or RAC3. Furthermore, all of the amino acid residues of RAC1 or RAC2 found to be mutated in cancer (Table S3) are completely conserved among RAC1, RAC2, and RAC3. Thus, transforming RAC3 mutants with similar nonsynonymous mutations may also exist in human cancer, although such mutations were not detected in the current screening. Of interest, none of the frequent mutation sites in RAS family proteins (G12, G13, and Q61) were found to be affected in RAC1 or RAC2, although an artificial G12V mutant of RAC1 did manifest constitutive GTP loading and transforming potential. Given that RAC proteins perform intracellular functions (such as orchestration of the actin cytoskeleton) that are distinct from those of RAS family members, RAC-driven activation of specific intracellular pathways may be advantageous for cancer development in vivo.

Given that we detected activation mutations of RAC1 or RAC2 in cell lines from sarcoma (HT1080), triple-negative breast cancer (MDA-MB-157 and HCC1143), and the blast crisis stage of CML (KCL-22), we performed deep sequencing of *RAC1*, *RAC2*, and *RAC3* cDNAs with GAIIx for specimens of triple-negative breast cancer (n = 66), of *RAC1* and *RAC2* cDNAs for specimens of CML in blast crisis (n = 43), and of *BCR-ABL1*–positive acute lymphoblastic leukemia (n = 31), as well as of *RAC1* cDNAs for specimens of sarcoma (n = 53). We failed, however, to detect any nonsynonymous mutations among these RAC cDNAs.

Our results have shown that RAC proteins have the potential to become oncogenic through amino acid substitution in a wide array of cancers. Although such RAC mutations may occur at a low frequency, the recent studies of Krauthammer et al. (22) and Hodis et al. (24) suggest that they may be enriched in melanoma (~5%). Importantly, given that HT1080 cells are highly addicted to the increased activity of RAC1(N92I), the targeting of oncogenic RAC proteins or their downstream effectors with small compounds or RNAi may prove to be an effective approach to the treatment of cancer harboring such oncoproteins.

Materials and Methods

The human fibrosarcoma cell line HT1080 was obtained from American Type Culture Collection, and subjected to deep sequencing with GAIIx. Recombinant retrovirus expressing the wild-type or mutant forms of RAC1 or RAC2 was used to infect mouse 3T3 fibroblasts to examine its transforming potential. Detailed information for cDNA resequencing, transformation assays, biochemical analysis of RAC proteins, and RNAi are detailed in *SI Materials and Methods*.

ACKNOWLEDGMENTS. This study was supported in part by a grant for Research on Human Genome Tailor-Made from the Ministry of Health, Labor, and Welfare of Japan; Grants-in-Aid for Scientific Research (B) from the Japan Society for the Promotion of Science; and grants from The Yasuda Medical Foundation, The Sagawa Foundation for Promotion of Cancer Research, and The Mitsubishi Foundation.

1. Druker BJ, et al.; IRIS Investigators (2006) Five-year follow-up of patients receiving imatinib for chronic myeloid leukemia. *N Engl J Med* 355(23):2408–2417.
2. Soda M, et al. (2007) Identification of the transforming *EML4-ALK* fusion gene in non-small-cell lung cancer. *Nature* 448(7153):561–566.
3. Shaw AT, et al. (2011) Effect of crizotinib on overall survival in patients with advanced non-small-cell lung cancer harbouring ALK gene rearrangement: A retrospective analysis. *Lancet Oncol* 12(11):1004–1012.
4. Colicelli J (2004) Human RAS superfamily proteins and related GTPases. *Sci STKE* 2004 (250):RE13.
5. Cox AD, Der CJ (2010) Ras history: The saga continues. *Small GTPases* 1(1):2–27.
6. Jaffee EM, Hruban RH, Canto M, Kern SE (2002) Focus on pancreas cancer. *Cancer Cell* 2(1):25–28.
7. Wertheimer E, et al. (2012) Rac signaling in breast cancer: A tale of GEFs and GAPs. *Cell Signal* 24(2):353–362.
8. Ridley AJ, Paterson HF, Johnston CL, Diekmann D, Hall A (1992) The small GTP-binding protein rac regulates growth factor-induced membrane ruffling. *Cell* 70(3):401–410.
9. Qiu RG, Chen J, Kirn D, McCormick F, Symons M (1995) An essential role for Rac in Ras transformation. *Nature* 374(6521):457–459.
10. Senger DL, et al. (2002) Suppression of Rac activity induces apoptosis of human glioma cells but not normal human astrocytes. *Cancer Res* 62(7):2131–2140.
11. Thomas EK, et al. (2007) Rac guanosine triphosphatases represent integrating molecular therapeutic targets for BCR-ABL-induced myeloproliferative disease. *Cancer Cell* 12(5):467–478.
12. Rasheed S, Nelson-Rees WA, Toth EM, Arnstein P, Gardner MB (1974) Characterization of a newly derived human sarcoma cell line (HT-1080). *Cancer* 33(4):1027–1033.
13. Ueno T, et al. (2012) High-throughput resequencing of target-captured cDNA in cancer cells. *Cancer Sci* 103(1):131–135.
14. Hall A, Marshall CJ, Spurr NK, Weiss RA (1983) Identification of transforming gene in two human sarcoma cell lines as a new member of the ras gene family located on chromosome 1. *Nature* 303(5916):396–400.
15. Debnath J, Muthuswamy SK, Brugge JS (2003) Morphogenesis and oncogenesis of MCF-10A mammary epithelial acini grown in three-dimensional basement membrane cultures. *Methods* 30(3):256–268.
16. Hill CS, Wynne J, Treisman R (1995) The Rho family GTPases RhoA, Rac1, and CDC42Hs regulate transcriptional activation by SRF. *Cell* 81(7):1159–1170.
17. Marshall CJ, Hall A, Weiss RA (1982) A transforming gene present in human sarcoma cell lines. *Nature* 299(5879):171–173.
18. Adari H, Lowy DR, Willumsen BM, Der CJ, McCormick F (1988) Guanosine triphosphatase activating protein (GAP) interacts with the p21 ras effector binding domain. *Science* 240(4851):518–521.
19. Calés C, Hancock JF, Marshall CJ, Hall A (1988) The cytoplasmic protein GAP is implicated as the target for regulation by the ras gene product. *Nature* 332(6164): 548–551.
20. Reinstein J, Schlichting I, Frech M, Goody RS, Wittinghofer A (1991) p21 with a phenylalanine 28——leucine mutation reacts normally with the GTPase activating protein GAP but nevertheless has transforming properties. *J Biol Chem* 266(26): 17700–17706.
21. Lin R, Bagrodia S, Cerione R, Manor D (1997) A novel Cdc42Hs mutant induces cellular transformation. *Curr Biol* 7(10):794–797.
22. Krauthammer M, et al. (2012) Exome sequencing identifies recurrent somatic RAC1 mutations in melanoma. *Nat Genet* 44(9):1006–1014.
23. Paterson H, et al. (1987) Activated N-ras controls the transformed phenotype of HT1080 human fibrosarcoma cells. *Cell* 51(5):803–812.
24. Hodis E, et al. (2012) A landscape of driver mutations in melanoma. *Cell* 150(2): 251–263.

DM Ross[1,2], M O'Hely[3], PA Bartley[2], P Dang[1], J Score[4], JM Goyne[1], M Sobrinho-Simoes[5,6], NCP Cross[4], JV Melo[1,6], TP Speed[3], TP Hughes[1] and AA Morley[2]
[1]*Department of Haematology, Centre for Cancer Biology, SA Pathology and University of Adelaide, Adelaide, South Australia, Australia;*
[2]*Department of Haematology and Genetic Pathology, Flinders University and Medical Centre, Adelaide, South Australia, Australia;*
[3]*Department of Bioinformatics, Walter and Eliza Hall Institute, Melbourne, Victoria, Australia;*
[4]*Faculty of Medicine, Wessex Regional Genetics Laboratory, Salisbury District Hospital, University of Southampton, Salisbury, UK;*
[5]*Department of Clinical Hematology, Hospital S João, Medical Faculty of the University of Porto, Porto, Portugal and*
[6]*Department of Haematology, Imperial College, London, UK*
Email: david.ross@health.sa.gov.au

REFERENCES

1 Gillert E, Leis T, Repp R, Reichel M, Hosch A, Breitenlohner I *et al.* A DNA damage repair mechanism is involved in the origin of chromosomal translocations t(4;11) in primary leukemic cells. *Oncogene* 1999; **18**: 4663–4671.
2 Reiter A, Saussele S, Grimwade D, Wiemels JL, Segal MR, Lafage-Pochitaloff M *et al.* Genomic anatomy of the specific reciprocal translocation t(15;17) in acute promyelocytic leukemia. *Genes Chromosomes Cancer* 2003; **36**: 175–188.
3 Zhang JG, Goldman JM, Cross NC. Characterization of genomic BCR-ABL breakpoints in chronic myeloid leukaemia by PCR. *Br J Haematol* 1995; **90**: 138–146.
4 Mattarucchi E, Guerini V, Rambaldi A, Campiotti L, Venco A, Pasquali F *et al.* Microhomologies and interspersed repeat elements at genomic breakpoints in chronic myeloid leukemia. *Genes Chromosomes Cancer* 2008; **47**: 625–632.
5 Jeffs AR, Benjes SM, Smith TL, Sowerby SJ, Morris CM. The BCR gene recombines preferentially with Alu elements in complex BCR-ABL translocations of chronic myeloid leukaemia. *Hum Mol Genet* 1998; **7**: 767–776.
6 Krumbholz M, Karl M, Tauer JT, Thiede C, Rascher W, Suttorp M *et al.* Genomic BCR-ABL1 breakpoints in pediatric chronic myeloid leukemia. *Genes Chromosomes Cancer* 2012; **51**: 1045–1053.
7 Score J, Calasanz MJ, Ottman O, Pane F, Yeh RF, Sobrinho-Simoes MA *et al.* Analysis of genomic breakpoints in p190 and p210 BCR-ABL indicate distinct mechanisms of formation. *Leukemia* 2010; **24**: 1742–1750.
8 Bartley PA, Martin-Harris MH, Budgen BJ, Ross DM, Morley AA. Rapid isolation of translocation breakpoints in chronic myeloid and acute promyelocytic leukaemia. *Br J Haematol* 2010; **149**: 231–236.
9 Sobrinho-Simoes M, Wilczek V, Score J, Cross NC, Apperley JF, Melo JV. In search of the original leukemic clone in chronic myeloid leukemia patients in complete molecular remission after stem cell transplantation or imatinib. *Blood* 2010; **116**: 1329–1335.
10 Ross DM, Schafranek L, Hughes TP, Nicola M, Branford S, Score J. Genomic translocation breakpoint sequences are conserved in BCR-ABL1 cell lines despite the presence of amplification. *Cancer Genet Cytogenet* 2009; **189**: 138–139.
11 Rahman M, Pearson LM, Heien HCA. Modified Anderson-Darling Test for Uniformity. *Bull Malays Math Sci Soc* 2006; **29**: 11–16.
12 Bailey TL, Boden M, Buske FA, Frith M, Grant CE, Clementi L *et al.* MEME SUITE: tools for motif discovery and searching. *Nucleic Acids Res* 2009; **37**: W202–W208.
13 Kato T, Inagaki H, Kogo H, Ohye T, Yamada K, Emanuel BS *et al.* Two different forms of palindrome resolution in the human genome: deletion or translocation. *Hum Mol Genet* 2008; **17**: 1184–1191.
14 Saglio G, Storlazzi CT, Giugliano E, Surace C, Anelli L, Rege-Cambrin G *et al.* A 76-kb duplicon maps close to the BCR gene on chromosome 22 and the ABL gene on chromosome 9: possible involvement in the genesis of the Philadelphia chromosome translocation. *Proc Natl Acad Sci USA* 2002; **99**: 9882–9887.
15 Ross DM, Branford S, Seymour JF, Schwarer AP, Arthur C, Bartley PA *et al.* Patients with chronic myeloid leukemia who maintain a complete molecular response after stopping imatinib treatment have evidence of persistent leukemia by DNA PCR. *Leukemia* 2010; **24**: 1719–1724.

Supplementary Information accompanies this paper on the Leukemia website (http://www.nature.com/leu)

Computational dissection of distinct microRNA activity signatures associated with peripheral T cell lymphoma subtypes

Leukemia (2013) **27**, 2107–2111; doi:10.1038/leu.2013.121

In hematological malignancies, various studies on microRNA (miRNA) profiling have highlighted specific miRNA signatures associated with several clinical conditions, such as disease subtypes, drug responses, and clinical outcomes in leukemia and B cell lymphomas, in parallel with the mRNA profiling study.[1,2] On the other hand, the characterization of these disease-related miRNA signatures is often compromised by the poor overlapping results of multiple independent studies, even if they focused on the same disease.[3,4] This problem may be partly explained by a poor overlap among differentially expressed miRNAs identified by multiple miRNA microarray platforms.[4] One promising approach is the paired profiling of mRNAs and miRNAs, and integrated analysis of both to extract disease-related features. Although the pairing of miRNAs and target mRNAs can be inferred from anticorrelation between miRNAs and mRNAs, the generally weak impacts of miRNAs on mRNA expression levels still make this approach difficult.

To this end, we have recently developed GSEA–FAME analysis (GFA) through combining GSEA and FAME to consider weak mRNA changes and the variability of the strength of correlations between an miRNA and its target genes.[5] GFA utilizes mRNA expression profiling to predict alterations in miRNA activities through rank-based enrichment analysis and evaluation of weighted miRNA–mRNA interactions (Figure 1a).[5] We demonstrated that GFA is useful for the assessment of widespread correlations between miRNA expression levels and miRNA activity status in diffuse large B cell lymphoma, and that GFA-based inference of miRNA activity improves the extraction of prognostic miRNAs by miRNA profiling in TCGA glioblastoma data set.[5] In this report, we applied this analysis to the gene expression profiling of peripheral T cell lymphomas (PTCL), in which the roles of miRNAs have not been well investigated, and made a prediction map of differential miRNA activities.

Recent miRNA profiling in anaplastic large cell lymphoma (ALCL) showed dysregulated miRNA profiles, including miR-17–92 cluster, miR-106a and miR-155, between anaplastic lymphoma kinase (ALK)+ and ALK− ALCLs.[6] In addition, we and another group reported miR-135b upregulation and miR-29a

Accepted article preview online 18 April 2013; advance online publication, 10 May 2013

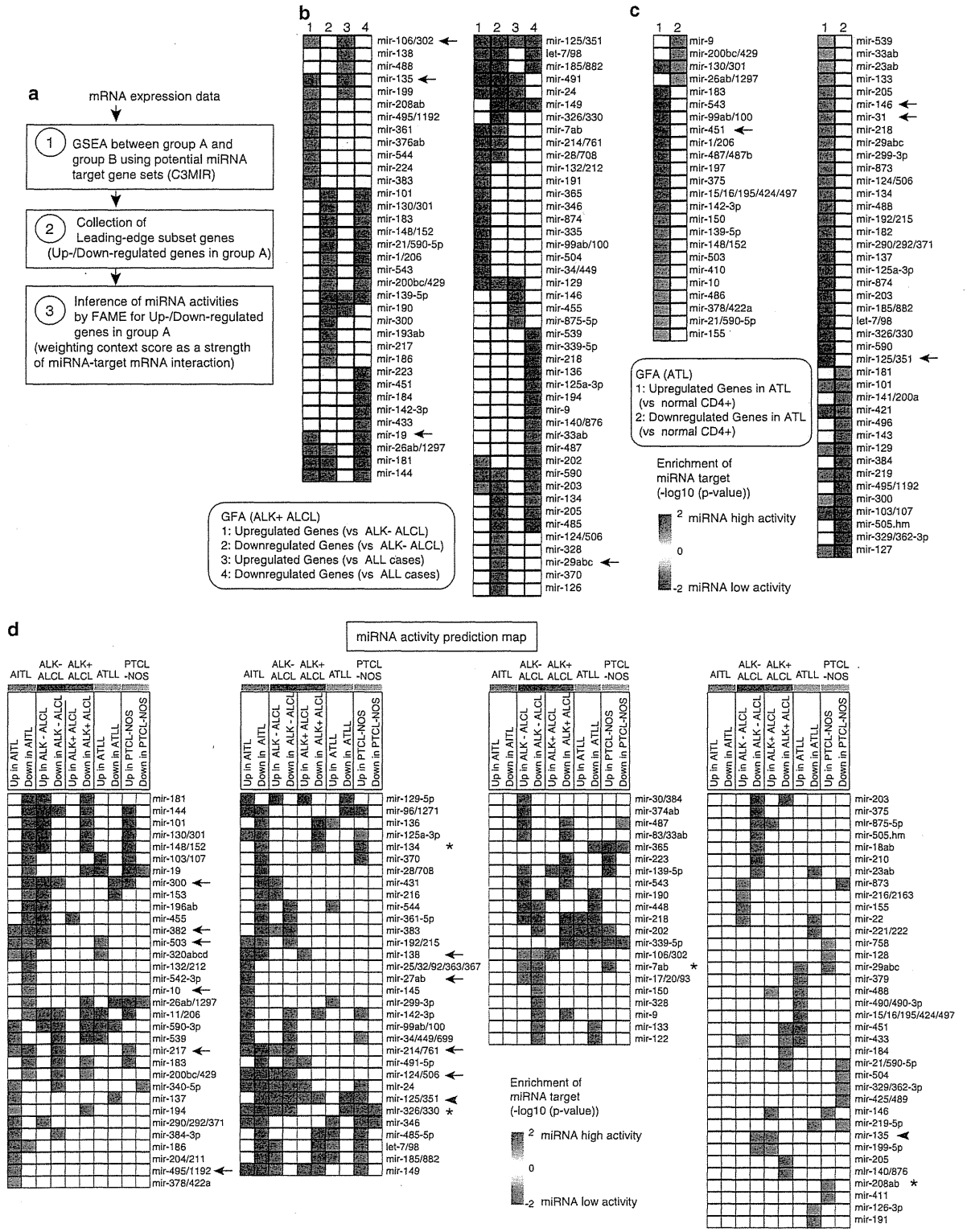

Figure 1. Prediction of miRNA activities in peripheral T cell lymphoma by GFA. (**a**) Outline of GFA. The details of GFA have been described in Supplementary Information. (**b**) GFA in ALK+ ALCL. GFA was performed between ALK+ and ALK− ALCL, and between ALK+ ALCL and all cases of PTCL in the gene expression profile of T cell lymphoma (GSE19069). miRNAs with $P > 0.05$ are shown as white squares. miRNAs indicated by arrows have been discussed in the main text. (**c**) GFA in ATL. GFA was performed between ATL cells and CD4-positive normal T cells in the gene expression profile of ATL (GSE33615). miRNAs with $P > 0.1$ are shown as white squares. miRNAs indicated by arrows have been discussed in the main text. (**d**) GFA in PTCL subtypes. For four major T cell lymphoma subtypes (AITL, ALK+ ALCL, ATLL and PTCL-NOS), GFA was performed between each lymphoma subtype and all cases of PTCL in GSE19069 data set. miRNAs with $P > 0.05$ are shown as white squares. miRNAs indicated by arrows (for AITL), arrowheads (for ALK+ ALCL and ATLL) and asterisks (for PTCL-NOS) have been discussed in the main text.

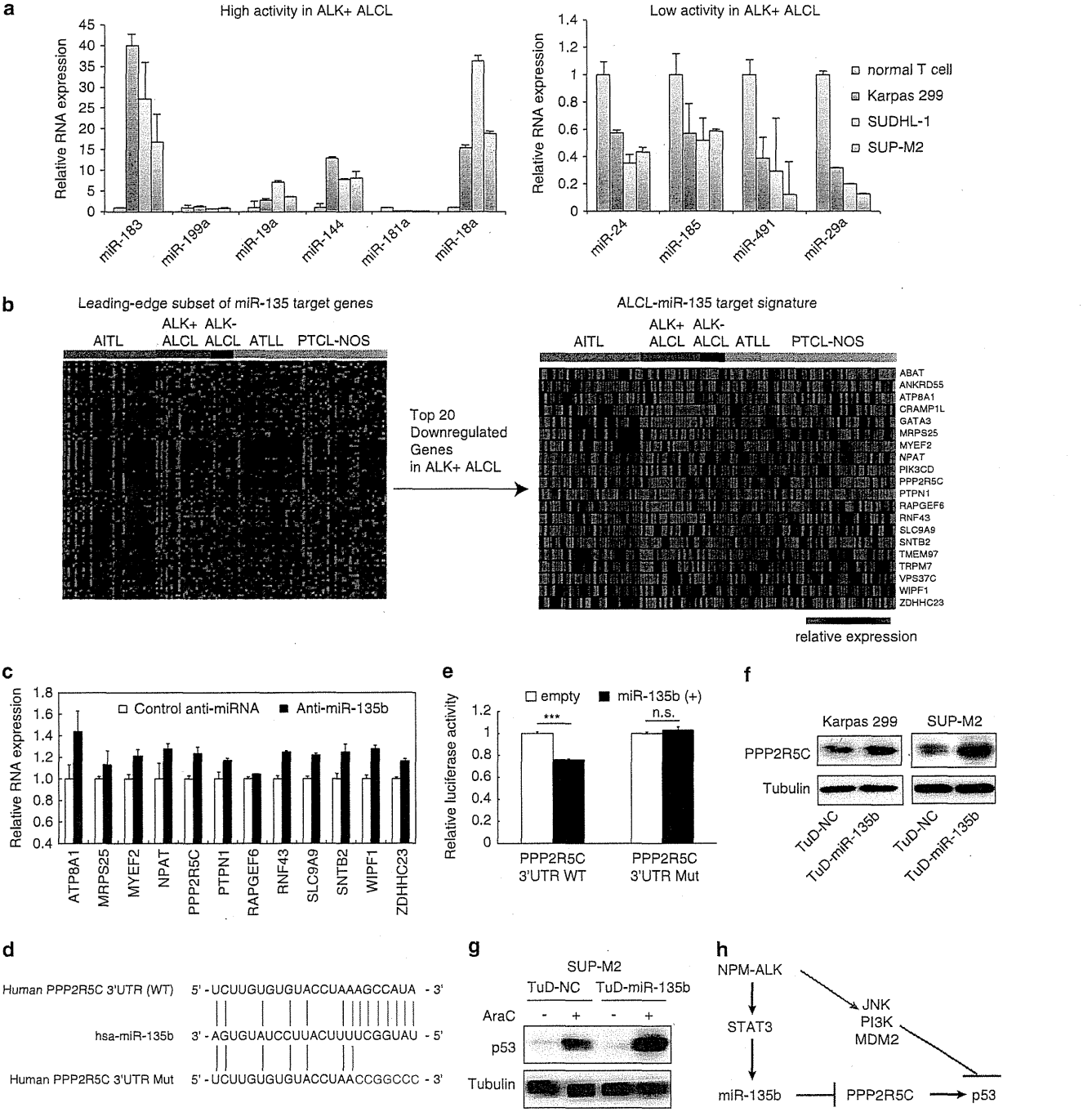

Figure 2. Validation of GFA results and identification of miR-135b–PPP2R5C–p53 axis in ALK+ ALCL. (**a**) Expression of mature miR-183, -199a, -19a, -144, -181a, -18a, -24, -185, -491 and -29a in normal T lymphocytes and NPM–ALK+ ALCL cell lines (Karpas 299, SUDHL-1 and SUP-M2), detected by qRT-PCR analysis. (**b**) ALCL–miR-135 target signature. Among the leading-edge gene set of miR-135 target genes (left) in GFA, the top 20 downregulated genes in ALK+ ALCL compared with other lymphoma subtypes were extracted as highly potential miR-135b target genes (ALCL–miR-135 target signature) in ALK+ ALCL (right). (**c**) Effects of miR-135b inhibition on mRNA expression levels of ALCL–miR-135 target genes in Karpas 299 cells. After transfection with miRNA inhibitors, Karpas 299 cells were subjected to qRT-PCR analysis. (**d**) Sequence alignment between miR-135b and its putative binding sites in PPP2R5C 3′-untranslated region (UTR). (**e**) miR-135b targets PPP2R5C. Luciferase activity of the PPP2R5C 3′-UTR reporter constructs with the wild-type or mutated target site (shown in (**d**)) in HEK293T cells co-transfected with an empty vector or pri-miR-135b expression vector (miR-135b (+)). $^{***}P<0.001$; n.s., not significant. (**f**) Elevated expression of PPP2R5C protein by miR-135b inhibition in ALCL cells. Karpas 299 and SUP-M2 cells were infected with lentivirus harboring TuD-NC or TuD–miR-135b, and applied to immunoblot analysis. (**g**) Enhancement of DNA damage-mediated p53 induction by miR-135b suppression in SUP-M2 cells. SUP-M2 cells were infected with lentivirus harboring TuD-NC or TuD–miR-135b, treated by AraC (1 μM, 24 h), and applied to immunoblot analysis. (**h**) Suppression of the p53 pathway by NPM–ALK–miR-135b–PPP2R5C axis. Green lines indicate alternative cascades connecting NPM–ALK to the inhibition of p53 activities shown in other study.[14]

downregulation in ALK+ ALCL, respectively.[7,8] We used the results of comprehensive gene expression profiling on 144 PTCL patients, including AITL, ALK+ ALCL, ALK− ALCL, adult T cell leukemia/lymphoma (ATLL) and PTCL not-otherwise-specified (PTCL-NOS).[9] We performed GFA between ALK+ ALCL and ALK− ALCL, and between ALK+ ALCL and all PTCL cases so that GFA could be applied for more than two groups. GFA results successfully predicted high activity of miR-106 and miR-135 and low activity of miR-29 in ALK+ ALCL both in comparison with ALK− ALCL and with all cases (Figure 1b). In miR-17–92 cluster, miR-19 was predicted to be active.

Recently published miRNA and mRNA profiling in the primary clinical samples of adult T cell leukemia (ATL) highlighted the loss of miR-31 in ATL.[10] GFA applied to this data set consistently showed low miR-31 activity in ATL (Figure 1c). GFA results also highlighted altered activities of several miRNAs such as miR-125 (low), miR-146 (low) and miR-451 (high), which matched the results of miRNA expression profiling in this data set.

As summarized in Figure 1d, GFA for five PTCL subtypes showed the characteristic patterns of different miRNA activities in distinct lymphoma subtypes. For example, miR-10, -217, -300, -382, -495 and -503 were predicted to be active in AITL (Figure 1d, Arrows). Conversely, miR-27, -124, -138 and -214 were predicted to be underactive in AITL (Figure 1d, Arrows). GFA showed high activity of miR-135 specifically in ALK+ ALCL, and low activity of miR-125 in ATLL (Figure 1d, Arrowhead). The different results for ATLL in Figures 1c and d may be due to the heterogeneity in the clinical entities of ATLL, differences in comparison targets (normal CD4 T cells and other subtypes) and low tumor content in clinical samples.

In PTCL-NOS, several miRNAs such as miR-326 and -134 were predicted to be active, and other miRNAs including miR-7 and -208 were predicted to be underactive (Figure 1d, Asterisks). It has been recently shown that the most upregulated (miR-326, -663b and -711) and downregulated (miR-203 and -205) miRNAs in cutaneous T cell lymphoma distinguish cutaneous T cell lymphoma and PTCL-NOS from benign skin diseases.[11] Among these miRNAs, GFA predicted high activity of miR-326 with a $P<0.05$ threshold, and low activity of miR-205 with a $P<0.1$ threshold. This implies that these miRNAs may also be useful for the classification of PTCL-NOS and other lymphoma subtypes, in addition to the separation of PTCL-NOS from benign diseases. These results indicate a good correlation between the alteration in miRNA expression levels directly measured in the literature and changes in miRNA activities inferred from independent published gene expression profiling, suggesting that GFA can predict biologically relevant changes in miRNA activities from mRNA profiling. As global miRNA profiling has not been reported in PTCL, this prediction should be assessed further in future investigations. Differences in tumor content in clinical samples, especially low content in AITL and PTCL-NOS, should be also considered for interpretation.

We next investigated whether mRNA profiling can be utilized for reverse identification of disease-related miRNAs and target identification of disease-related miRNAs. We investigated the expression levels of GFA-supported miRNAs in ALK+ ALCL. As shown in Figure 2a, high expression of miR-183, -18a and -19a was confirmed in three ALCL cell lines harboring *NPM–ALK* fusion; Karpas 299, SUDHL-1 and SUP-M2 cells, relative to normal T cells. In addition to miR-29a, downregulation of miR-24, -185 and -491 was also observed. Furthermore, upregulation of miR-183, -18a and -19a was confirmed in human primary ALK+ ALCL samples, relative to reactive lymph node and ALK− ALCL samples (Supplementary Figure S1). Interestingly, we observed no significant changes in miR-199a and miR-181a in the cell lines, but these miRNAs were upregulated in clinical samples (Figure 2a and Supplementary Figure S1). Considering that GFA is based on the expression profiling of clinical samples, the upregulation of miR-199a and miR-181a may be attributable to the *in vivo* reaction in ALCL.

GFA generates a list of probable target genes for each miRNA for further convenient experimental validation of miRNA–mRNA interactions. Consistent with our report,[8] GFA revealed that high miR-135b activity seems to leave its footprint on clinical ALCL transcriptome. Among the leading-edge gene subset of potential miR-135 target genes that were downregulated in ALK+ ALCL, the top 20 downregulated genes (referred to as 'ALCL–miR-135 target signature') included several genes such as *GATA3*, *PPP2R5C* and *RAPGEF6* (Figure 2b). Our previous report showed that GATA3 is a direct target of miR-135b in ALCL. We observed that a large proportion of the 'ALCL–miR-135 target signature' (ATP8A1, MRPS25, MYEF2, NPAT, PPP2R5C, PTPN1, RAPGEF6, RNF43, SLC9A9, SNTB2, WIPF1 and ZDHHC23) was indeed upregulated by miR-135b inhibition in Karpas 299 ALCL cells (Figure 2c), suggesting the direct contribution of miR-135b to the downregulation of the 'ALCL–miR-135 target signature' in ALCL. We defined a deregulation index for target gene sets by averaging normalized gene expression values and investigated the association between the 'ALCL–miR-135 target signature', which potentially reflects miR-135b activity, and interleukin-17-producing immunophenotype rendered by miR-135b overexpression in ALCL.[8] The deregulation index values of the 'ALCL–miR-135 target signature' and Th17-related genes were clearly low and high in ALK+ ALCL, respectively (Supplementary Figure S2a), and these two values showed a negative correlation (Supplementary Figure S2b). Comparable results were confirmed in another data set for T cell lymphoma (Supplementary Figure S2c).[12] Similar approach also suggested the potential interaction between miR-125 with low activity in ATLL and several known targets, including IRF4, IKZF4, KLF13, ETS1, ARID3B and MCL1 (Supplementary Figure S3).

Although molecular functions are largely unknown in most 'ALCL–miR-135 target signature' genes, we focused on PPP2R5C, which encodes protein phosphatase 2A (PP2A) regulatory subunit B56γ, as PP2A B56γ mediates the DNA-damage-induced dephosphorylation and stabilization of p53, and thus exerts a tumor-suppressor function.[13] Exogenous miR-135b suppressed the translational efficiency of PPP2R5C 3′-untranslated region depending on the target site (Figures 2d and e). Knockdown of miR-135b by TuD RNA increased the protein expression levels of PPP2R5C in ALCL cells (Figure 2f), indicating PPP2R5C as an endogenous miR-135b target. Consistent with the positive effect of PPP2R5C on p53, miR-135b inhibition enhanced p53 accumulation by the DNA damaging agent AraC in p53-wild-type SUP-M2 cells (Figure 2g). Therefore, NPM–ALK may suppress p53 activity through miR-135b–PPP2R5C axis, and upregulation of MDM2 and JNK activities reported previously[14] (Figure 2h).

Our findings reinforce the possibility of inference of miRNA regulation underlying the mRNA profiles from numerous gene expression data sets in publicly accessible repositories, even if these studies included one-sided mRNA profiles and did not design miRNA profiling. The results in Figures 2b and c; and Supplementary Figure S2 suggest that a subset of miRNA target genes can represent the biological activity of corresponding miRNAs. Png *et al.*[15] recently showed similar approach, in which eight miR-126 target genes reflect the metastasis-suppressor activity of miR-126 and strongly correlate with metastatic relapse in human breast cancer. GFA may be useful for the identification of such representative miRNA target genes. The present study suggests that combinational investigation of gene expression profiling and computational miRNA activity predictions may yield a wide platform for assessment of miRNA involvement in various disease processes, together with miRNA profiling.

CONFLICT OF INTEREST

The authors declare no conflict of interest.

ACKNOWLEDGEMENTS

We thank Nishimori H, Morishita Y and Mihira H for their discussion and skilled technical assistance; and all the members of the Department of Molecular Pathology, the University of Tokyo. This work was supported by KAKENHI (Grants-in-Aid for Young Scientists (A) (no. 24689018) and for Scientific Research on Innovative Areas 'RNA regulation' (no. 23112702), and 'Integrative research on cancer microenvironment network' (no. 22112002)), the Global Center of Excellence Program for 'Integrative Life Science Based on the Study of Biosignaling Mechanisms' from the Ministry of Education, Culture, Sports, Science, and Technology of Japan, and the Cell Science Research Foundation.

AUTHOR CONTRIBUTIONS

HIS designed the research, performed experiments and analyses, and wrote the paper; HM provided the key materials, and performed the experiments and analyses; MN, TY, NK and KS provided clinical samples; and KS and KM supervised the project and wrote the paper.

HI Suzuki[1], H Matsuyama[1], M Noguchi[2], T Yao[3], N Komatsu[4], H Mano[5,6], K Sugimoto[4,7] and K Miyazono[1]

[1]Department of Molecular Pathology, Graduate School of Medicine, The University of Tokyo, Bunkyo-ku, Japan;
[2]Department of Hematology, Juntendo Urayasu Hospital, Urayasu-shi, Japan;
[3]Department of Human Pathology, Juntendo University Graduate School of Medicine, Bunkyo-ku, Japan;
[4]Division of Hematology, Department of Internal Medicine, Juntendo University Graduate School of Medicine, Bunkyo-ku, Japan;
[5]Department of Medical Genomics, Graduate School of Medicine, The University of Tokyo, Bunkyo-ku, Japan;
[6]Division of Functional Genomics, Jichi Medical University, Shimotsuke-shi, Japan and
[7]Department of Hematology and Oncology, JR Tokyo General Hospital, Shibuya-ku, Japan
E-mail: hisuzuki-tky@umin.ac.jp or miyazono@m.u-tokyo.ac.jp

REFERENCES

1 Schotte D, Pieters R, Den Boer ML. MicroRNAs in acute leukemia: from biological players to clinical contributors. *Leukemia* 2012; **26**: 1–12.
2 Akbari Moqadam F, Pieters R, den Boer ML. The hunting of targets: challenge in miRNA research. *Leukemia* 2013; **27**: 16–23.
3 Pritchard CC, Cheng HH, Tewari M. MicroRNA profiling: approaches and considerations. *Nat Rev Genet* 2012; **13**: 358–369.
4 Callari M, Dugo M, Musella V, Marchesi E, Chiorino G, Grand MM *et al.* Comparison of microarray platforms for measuring differential microRNA expression in paired normal/cancer colon tissues. *PLoS One* 2012; **7**: e45105.
5 Suzuki HI, Mihira H, Watabe T, Sugimoto K, Miyazono K. Widespread inference of weighted microRNA-mediated gene regulation in cancer transcriptome analysis. *Nucleic Acids Res* 2013; **41**: e62.
6 Merkel O, Hamacher F, Laimer D, Sifft E, Trajanoski Z, Scheideler M *et al.* Identification of differential and functionally active miRNAs in both anaplastic lymphoma kinase (ALK)+ and ALK- anaplastic large-cell lymphoma. *Proc Natl Acad Sci USA* 2010; **107**: 16228–16233.
7 Desjobert C, Renalier MH, Bergalet J, Dejean E, Joseph N, Kruczynski A *et al.* MiR-29a down-regulation in ALK-positive anaplastic large cell lymphomas contributes to apoptosis blockade through MCL-1 overexpression. *Blood* 2011; **117**: 6627–6637.
8 Matsuyama H, Suzuki HI, Nishimori H, Noguchi M, Yao T, Komatsu N *et al.* miR-135b mediates NPM-ALK-driven oncogenicity and renders IL-17-producing immunophenotype to anaplastic large cell lymphoma. *Blood* 2011; **118**: 6881–6892.
9 Iqbal J, Weisenburger DD, Greiner TC, Vose JM, McKeithan T, Kucuk C *et al.* Molecular signatures to improve diagnosis in peripheral T-cell lymphoma and prognostication in angioimmunoblastic T-cell lymphoma. *Blood* 2010; **115**: 1026–1036.
10 Yamagishi M, Nakano K, Miyake A, Yamochi T, Kagami Y, Tsutsumi A *et al.* Polycomb-mediated loss of miR-31 activates NIK-dependent NF-kappaB pathway in adult T cell leukemia and other cancers. *Cancer Cell* 2012; **21**: 121–135.
11 Ralfkiaer U, Hagedorn PH, Bangsgaard N, Lovendorf MB, Ahler CB, Svensson L *et al.* Diagnostic microRNA profiling in cutaneous T-cell lymphoma (CTCL). *Blood* 2011; **118**: 5891–5900.
12 Piccaluga PP, Agostinelli C, Califano A, Rossi M, Basso K, Zupo S *et al.* Gene expression analysis of peripheral T cell lymphoma, unspecified, reveals distinct profiles and new potential therapeutic targets. *J Clin Invest* 2007; **117**: 823–834.
13 Li HH, Cai X, Shouse GP, Piluso LG, Liu X. A specific PP2A regulatory subunit, B56gamma, mediates DNA damage-induced dephosphorylation of p53 at Thr55. *EMBO J* 2007; **26**: 402–411.
14 Cui YX, Kerby A, McDuff FK, Ye H, Turner SD. NPM-ALK inhibits the p53 tumor suppressor pathway in an MDM2 and JNK-dependent manner. *Blood* 2009; **113**: 5217–5227.
15 Png KJ, Halberg N, Yoshida M, Tavazoie SF. A microRNA regulon that mediates endothelial recruitment and metastasis by cancer cells. *Nature* 2012; **481**: 190–194.

Supplementary Information accompanies this paper on the Leukemia website (http://www.nature.com/leu)

Leukemic evolution of donor-derived cells harboring *IDH2* and *DNMT3A* mutations after allogeneic stem cell transplantation

Leukemia (2014) **28,** 426–428; doi:10.1038/leu.2013.278

Although allogeneic stem cell transplantation is effective for the treatment of leukemia with poor prognosis, some such treated individuals experience disease relapse at various times after transplantation. Chimerism analysis of the relapsed disease has revealed infrequent cases in which the malignant cells originate from the donor and not from the initial leukemic clones.[1,2] Such donor cell leukemia (DCL) is often refractory to further treatment, with a mean overall survival for the affected patients of only 32.8 months.[2]

We recently described a 47-year-old Japanese man with acute myeloid leukemia (AML) who underwent a transplantation of peripheral blood stem cells (PBSCs) from his HLA-matched brother.[3] Although the allogeneic transplantation was successful, AML again became apparent in the patient 27 months later and chimerism analysis revealed that the leukemia was DCL. Genomic DNA was isolated and subjected to whole-exome sequencing from specimens of the initial AML (containing 70% myeloblasts, referred to as sample P1), the first complete remission after chemotherapy (sample P2), the first relapse (containing 24% myeloblasts; sample P3), donor PBSCs (sample D1), DCL at 27 months after allogeneic transplantation (containing 6% myeloblasts, sample D2) and DCL at 36 months after transplantation (containing 71% myeloblasts, sample D3).

Exome sequencing yielded a total of ~84.7 million, ~31.6 million, ~73.5 million, ~44.3 million and ~53.2 million unique, high-quality, paired-end reads for samples P1, P2, P3, D1 and D3, respectively (Supplementary Information). Although chimerism analysis for short tandem repeats had indicated that D3 was derived from D1 clones,[3] we further examined this possibility in a genome-wide manner. As demonstrated in Supplementary Figure 1a, the allele frequency of single-nucleotide polymorphisms (SNPs) detected in our data sets was highly concordant between P1 and P2 (Pearson's correlation coefficient (r) of 0.978) as well as between P1 and P3 ($r = 0.986$), suggesting that these three samples originate from a single individual. However, as expected, the concordance dropped substantially for the P1 and D3 pair ($r = 0.628$). In contrast, the concordance between D1 and D3 was high ($r = 0.983$), suggesting that the relapsed leukemia after transplantation was indeed derived from the donor cell. Of note, the allele frequency of SNPs showed only a low level of concordance ($r = 0.285$) between P1 and a cell line (KCL22)[4] derived from an unrelated Japanese patient with chronic myeloid leukemia (Supplementary Figure 1b). The correlation coefficient of 0.628 for P1 and D3 thus indicated that the patient and donor siblings share a substantial number of SNPs.

We next searched for somatic nonsynonymous mutations among the leukemic samples. For P1 and P3, we used P2 as a paired normal control. Given that D3 was shown to be derived from D1, we used the latter as the germline control for the former. Through our computational pipeline (Supplementary Information), nine missense mutations and two out-of-frame insertions/deletions (indels) were detected for P1, two missense mutations for P3 and nine missense mutations and one out-of-frame indel for D3 (Table 1). As described previously,[3] a 4-bp deletion of *CEBPA* was present in the initial AML but absent from the DCL. Similarly,

Table 1. Confirmed somatic mutations in the specimens analyzed

Specimen	*Gene symbol*	*GenBank accession no.*	*Nucleotide change*	*Amino-acid change*	*Mutation ratio (%)*				
					P1	*P2*	*P3*	*D1*	*D3*
P1	*ACSL5*	NM_016234	c.280G>A	p.V94I	40.6	0.0	30.6	0.0	0.0
	ANO4	NM_178826	c.2441C>T	p.S814L	42.3	0.0	16.7	0.0	0.0
	APOB	NM_000384	c.9175C>T	p.R3059C	32.8	0.0	7.4	0.0	0.0
	BANK1	NM_017935	c.222C>G	p.N74K	36.4	0.0	9.2	0.0	0.0
	CCDC88C	NM_001080414	c.3748G>A	p.E1250K	36.4	0.0	0.0	0.0	0.0
	FAM178B	NM_001122646	c.81G>A	p.M27I	41.2	0.0	25.0	0.0	0.0
	GABRB2	NM_021911	c.1009C>T	p.R337C	44.8	0.0	14.5	0.0	0.0
	JAK3	NM_000215	c.2570T>C	p.L857P	40.8	0.0	0.0	0.0	0.0
	SPATA31D1	NM_001001670	c.3793C>T	p.R1265C	36.6	0.0	6.7	0.0	0.0
	CEBPA	NM_004364	c.319_322delGACT	p.D107Tfs	63.6	0.0	10.0	0.0	0.0
	STAG2	NM_001042750	c.219_220insCG	p.H73Rfs	100.0	0.0	27.6	0.0	0.0
P3	*ACSL5*	NM_016234	c.280G>A	p.V94I	40.6	0.0	30.6	0.0	0.0
	NTNG2	NM_032536	c.1348G>T	p.G450C	0.0	0.0	37.5	0.0	0.0
D3	*CCDC168*	NM_001146197	c.11761G>C	p.D3921H	0.0	0.0	0.0	0.0	55.6
	GAL3ST1	NM_004861	c.1086G>T	p.M362I	0.0	0.0	0.0	0.0	32.6
	IDH2	NM_002168	c.419G>A	p.R140Q	0.0	0.0	0.0	7.1	50.0
	MYO7B	NM_001080527	c.635G>A	p.R212H	0.0	0.0	0.0	0.0	45.8
	NFATC1	NM_172390	c.736G>A	p.V246I	0.0	0.0	0.0	0.0	48.6
	PSMB8	NM_004159	c.637C>T	p.P213S	0.0	0.0	0.0	0.0	40.9
	TCAIM	NM_173826	c.668C>G	p.S223C	0.0	0.0	0.0	0.0	70.0
	TMEM132D	NM_133448	c.481G>A	p.A161T	0.0	0.0	0.0	0.0	35.3
	UBA2	NM_005499	c.419G>A	p.G140E	0.0	0.0	0.0	0.0	47.4
	DNMT3A	NM_153759	c.449delT	p.V150Gfs	0.0	0.0	0.0	8.7	61.1
	NRAS[a]	NM_002524	c.38G>A	p.G13D	0.0	0.0	0.0	0.0	18.4

[a]Below the threshold in the initial screening.

Accepted article preview online 26 September 2013; advance online publication, 15 October 2013

none of the identified somatic mutations were shared between the initial AML and DCL, providing further support for the distinct nature of the two leukemias.

Given that P3 contains only 24% myeloblasts, our computational pipeline could not accurately detect all of the associated somatic mutations. Indeed, most of the somatic mutations found in P1 (such as those in *ANO4*, *APOB*, *BANK1*, *STAG2* and *CEBPA*) were still present in P3 at lower frequencies (Table 1) but were not isolated in our pipeline analysis for P3. Lowering the threshold for somatic calls, however, increased the number of pseudopositive mutations in all specimens. We therefore applied the 30% threshold for mutation calls to all analyses. Of note, our data still indicate that P3 is not completely identical to P1. Nonsynonymous mutations of *CCDC88C* and *JAK3* detected in P1 were thus absent in P3, whereas a mutation of *NTNG2* was newly apparent in P3, suggestive of a clonal evolution in P3 divergent from the original P1 clones.

Surprisingly, whereas most somatic mutations detected in D3 were not present in D1, our results suggested that IDH2(R140Q) and DNMT3A(V150Gfs) were already present in the healthy donor at a low frequency (Table 1). Polymerase chain reaction (PCR)-based cloning of the genomic fragments and Sanger sequencing for *IDH2* and *DNMT3A* from D1 indeed confirmed the presence of the corresponding mutations in 2 (2.3%) out of 87 DNA clones and 1 (1.1%) out of 93 clones, respectively (Supplementary Figure 2). Furthermore, although the mutation rate (18.4%) was below the threshold of the present study, the oncogenic mutation NRAS(G13D)[5] in D3 (Table 1) was confirmed by Sanger sequencing of the corresponding genomic DNA (Supplementary Figure 2).

We then verified these infrequent mutations by sequencing the corresponding DNA fragments at extra-high coverage (hundreds of thousand times) with the use of a next-generation sequencer. The D2 sample, which contains only 6% myeloblasts, was also examined in this analysis. We confirmed that 1.6% (5.96×10^3 mutant reads out of 3.67×10^5 total reads at the corresponding nucleotide position) and 2.1% (1.24×10^4 out of 6.01×10^5 reads) of D1 cells already harbored the IDH2(R140Q) and DNMT3A(V150Gfs) mutations, respectively (Figure 1a). These mutations were not detected in the primary AML (P1 to P3). Whereas the *NRAS* mutation was not detected in D1, it became apparent in D2 and D3 at a frequency similar to that of the *IDH2* mutation. In addition, the *JAK3* mutation present in P1 was no longer evident at the relapsed stage P3.

On the basis of the genetic mutation profiles identified in the present case, we propose the following scheme for disease progression (Figure 1b). Given the high frequency of *STAG2* and *CEBPA* mutations in the primary AML, the 2-bp insertion in *STAG2* on the X chromosome (with there being only one copy of *STAG2* per cell in the male patient) as well as the heterozygous 4-bp deletion in *CEBPA* may characterize the founding clone of the original leukemia, with subsets of this clone subsequently acquiring additional oncogenic hits such as JAK3(L857P). The disappearance of *JAK3* and *CCDC88C* mutations in P3 suggests that the leukemic subclones harboring these mutations were sensitive to the initial chemotherapy.

The molecular pathogenesis of DCL has been unclear and may differ among cases. For instance, germline predisposition to cancer, such as the Li-Fraumeni syndrome or Bloom syndrome, may be shared between recipients and related donors.[6] However, in the present case, mutations in *IDH2* and *DNMT3A* were detected only in the donor, not in the primary AML, rendering this scenario unlikely. Alternatively, occult leukemia may already be present in the donor blood system and is inadvertently transmitted to the recipient.[7] In such cases, however, leukemia usually emerges in the donor soon after transplantation. Our donor, in contrast, has not developed any hematologic malignancy at 10 years after the donation of his PBSCs.

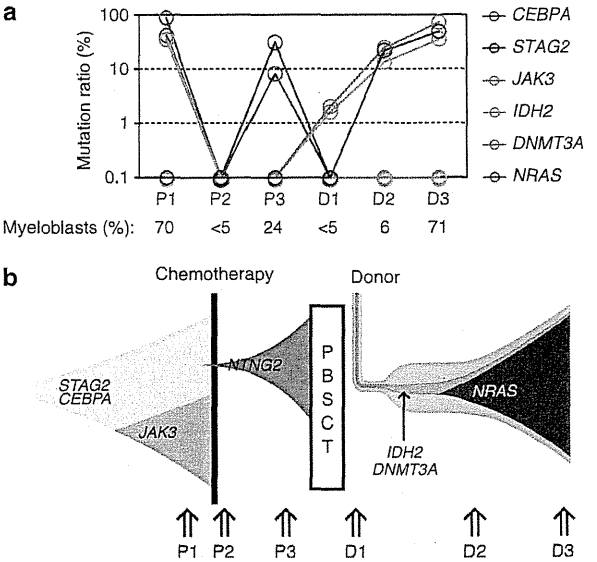

Figure 1. Genomic analysis of AML samples and donor PBSCs. (**a**) Genomic mutations corresponding to CEBPA(D107Tfs), STAG2(H73Rfs), JAK3(L857P), IDH2(R140Q), DNMT3A(V150Gfs) and NRAS(G13D) were examined by targeted deep sequencing in genomic DNA prepared from samples P1, P2, P3, D1, D2 and D3. The ratio of mutant reads to all reads at the corresponding position is shown as a percentage, with mutation frequencies of <0.1% being considered as 0.1% in the graph. The percentage of myeloblasts in each sample is indicated below the graph. (**b**) Founding clones of the primary AML harbored nonsynonymous mutations of *STAG2* and *CEBPA* and gave rise to subclones harboring a *JAK3* mutation. Whereas the latter cell population was sensitive to the initial chemotherapy, a subclone positive for an *NTNG2* mutation emerged from the former population and gave rise to relapse. All of these leukemic clones were successfully eradicated by peripheral blood stem cell transplantation (PBSCT). PBSCs of the donor, however, contained a small clonal population of cells positive for *IDH2* and *DNMT3A* mutations that eventually gave rise to AML on acquisition of additional mutations including NRAS(G13D).

Our present data therefore strongly suggest that apparently healthy individuals may harbor preleukemic subclones in their blood system (Figure 1b). Indeed, somatic mutations of *TET2* and *DNMT3A* were recently identified in clonal blood cells from one healthy elderly individual.[8] Furthermore, the *IDH2* and *DNMT3A* mutations identified in the present study may have had a specific role in the initiation of leukemia, given that mutations in the epigenetic modifiers including TET1/2, IDH1/2 and DNMT3A have been identified as early genetic events in AML progression.[9,10] Such mutations are indeed among the most frequently detected somatic alterations in AML.[11] These observations raise an important concern as to how 'appropriate' donors should be chosen, especially given that the incidence of DCL is increasing with the prevalence of molecular analysis for donor/recipient chimerism.[2] Prospective studies of whether and how examination of preleukemic subclones should be incorporated into the donor selection process for stem cell transplantation are thus warranted.

Furthermore, in our case, the oncogenic mutation NRAS(G13D) was likely a driver for leukemia progression, given that the frequency of this mutation was almost identical to that of the *IDH2* mutation in the D2 and D3 specimens. In contrast to the absence of leukemia in the donor, DCL rapidly developed in the recipient after transplantation in association with the accumulation of additional genetic hits, possibly as a result of a growth-promoting condition of the bone marrow after transplantation and due to a

defective immune surveillance resulting from the immunosuppressive treatment to control graft-versus-host disease.

CONFLICT OF INTEREST

The authors declare no conflict of interest.

ACKNOWLEDGEMENTS

This study was supported in part by a Grant-in-Aid from the Project for Development of Innovative Research on Cancer Therapeutics (P-Direct) from the Ministry of Education, Culture, Sports, Science and Technology of Japan and by grants for Third-Term Comprehensive Control Research for Cancer and for Research on Human Genome Tailor-made from the Ministry of Health, Labor and Welfare of Japan.

T Yasuda[1,2], T Ueno[1], K Fukumura[1], A Yamato[1], M Ando[1], H Yamaguchi[1], M Soda[1], M Kawazu[3], E Sai[3], Y Yamashita[3], M Murata[2], H Kiyoi[2], T Naoe[2,4] and H Mano[1,5]

[1]*Department of Cellular Signaling, Graduate School of Medicine, The University of Tokyo, Tokyo, Japan;*
[2]*Department of Hematology and Oncology, Graduate School of Medicine, Nagoya University, Aichi, Japan;*
[3]*Department of Medical Genomics, Graduate School of Medicine, The University of Tokyo, Tokyo, Japan;*
[4]*National Hospital Organization Nagoya Medical Center, Aichi, Japan and*
[5]*CREST, Japan Science and Technology Agency, Saitama, Japan*
E-mail: hmano@m.u-tokyo.ac.jp

REFERENCES

1 Fialkow PJ, Thomas ED, Bryant JI, Neiman PE. Leukaemic transformation of engrafted human marrow cells *in vivo*. *Lancet* 1971; **1**: 251–255.
2 Wiseman DH. Donor cell leukemia: a review. *Biol Blood Marrow Transplant* 2011; **17**: 771–789.
3 Murata M, Ishikawa Y, Ohashi H, Terakura S, Ozeki K, Kiyoi H *et al.* Donor cell leukemia after allogeneic peripheral blood stem cell transplantation: a case report and literature review. *Int J Hematol* 2008; **88**: 111–115.
4 Kubonishi I, Miyoshi I. Establishment of a Ph1 chromosome-positive cell line from chronic myelogenous leukemia in blast crisis. *Int J Cell Cloning* 1983; **1**: 105–117.
5 Prior IA, Lewis PD, Mattos C. A comprehensive survey of Ras mutations in cancer. *Cancer Res* 2012; **72**: 2457–2467.
6 Birch JM, Alston RD, McNally RJ, Evans DG, Kelsey AM, Harris M *et al.* Relative frequency and morphology of cancers in carriers of germline TP53 mutations. *Oncogene* 2001; **20**: 4621–4628.
7 Sala-Torra O, Hanna C, Loken MR, Flowers ME, Maris M, Ladne PA *et al.* Evidence of donor-derived hematologic malignancies after hematopoietic stem cell transplantation. *Biol Blood Marrow Transplant* 2006; **12**: 511–517.
8 Busque L, Patel JP, Figueroa ME, Vasanthakumar A, Provost S, Hamilou Z *et al.* Recurrent somatic *TET2* mutations in normal elderly individuals with clonal hematopoiesis. *Nat Genet* 2012; **44**: 1179–1181.
9 Jan M, Snyder TM, Corces-Zimmerman MR, Vyas P, Weissman IL, Quake SR *et al.* Clonal evolution of preleukemic hematopoietic stem cells precedes human acute myeloid leukemia. *Sci Transl Med* 2012; **4**: 149ra118.
10 Wakita S, Yamaguchi H, Omori I, Terada K, Ueda T, Manabe E *et al.* Mutations of the epigenetics-modifying gene (DNMT3a, TET2, IDH1/2) at diagnosis may induce FLT3-ITD at relapse in *de novo* acute myeloid leukemia. *Leukemia* 2013; **27**: 1044–1052.
11 Network TCGAR. Genomic and epigenomic landscapes of adult *de novo* acute myeloid leukemia. *N Engl J Med* 2013; **368**: 2059–2074.

Supplementary Information accompanies this paper on the Leukemia website (http://www.nature.com/leu)

Cytogenetics and outcome of infants with acute lymphoblastic leukemia and absence of *MLL* rearrangements

Leukemia (2014) **28,** 428–430; doi:10.1038/leu.2013.280

Acute lymphoblastic leukemia (ALL) in infants less than 1 year of age is rare and the biological features are different from ALL in older children.[1] Infant ALL is characterized by a high frequency of rearrangements of the *MLL* gene (*MLL*-R) and heterogeneous outcome. However overall, their event-free survival (EFS) is much worse than older children with ALL.[1–5] A large collaborative trial, Interfant-99, demonstrated improved outcome, while characterizing definitively the independent prognostic variables in infant ALL.[6] While cytogenetic data are reported within individual infant ALL clinical trials, the numbers are typically small and many reports are less detailed for those patients without *MLL* gene rearrangements (*MLL*-G). However, it was previously suggested that *MLL*-G had an important predictive influence on outcome.[7,8] These observations were later confirmed in Interfant-99,[6] in which *MLL*-G patients showed a threefold reduced risk of an event compared with *MLL*-R patients, although all *MLL*-G patients were grouped together into a single category. To better understand the association of different chromosomal abnormalities and outcome among *MLL*-G infants, here we have carried out detailed cytogenetic investigation of two infant ALL trials: Interfant-99 and Children's Oncology Group (COG)-P9407.

Patients were 365 days old or less with newly diagnosed ALL without a rearrangement of the *MLL* gene enrolled to Interfant-99 (May 1999–December 2005; $n=110$) and COG-P9407 (June 1996–October 2006; $n=52$).[6,9] Individual study groups obtained ethical approval, and treating physicians obtained informed consent from parents or guardians. The presence of *MLL* gene rearrangements was excluded using fluorescence *in situ* hybridization (FISH), reverse transcription (RT)-PCR and/or Southern blotting, as previously reported.[6] Each national study group provided patient data, including cytogenetics, FISH and molecular results. EFS and overall survival (OS) were calculated from the date of trial enrolement to the date of the first event (induction failure, relapse, second malignancy or death) or last follow-up. Median follow-up time was 7 years.

Among 162 *MLL*-G patients, no cytogenetic data were available for 34 (21%), resulting in a success rate of 79%. An abnormal karyotype was detected in 90/128 (70%) patients with a successful cytogenetic result (Supplementary Table 1) with the remainder classified as normal based on the presence of at least 10 (but usually 20) normal metaphases. They were categorized according to cytogenetic risk group as previously defined for childhood ALL.[10] Compared with childhood ALL (1–18 years) using data from the UKALL97/99 treatment trial,[10] the frequency of good risk cytogenetic abnormalities among *MLL*-G infants was significantly lower (12 vs 60%, $P<0.01$), whereas the frequency of poor risk abnormalities (excluding *MLL* translocations) was similar (8 vs 10%). Although *ETV6–RUNX1* fusion is present in 25% of childhood ALL, we found no *ETV6–RUNX1* cases among the 75 patients tested by FISH or RT-PCR. High hyperdiploidy (HeH) was the most

Accepted article preview online 27 September 2013; advance online publication, 25 October 2013

OPEN ACCESS

Open Access
Scan to access more free content

ORIGINAL ARTICLE

Impact of the Tohoku earthquake and tsunami on pneumonia hospitalisations and mortality among adults in northern Miyagi, Japan: a multicentre observational study

Hisayoshi Daito,[1,2] Motoi Suzuki,[3] Jun Shiihara,[1,2] Paul E Kilgore,[4] Hitoshi Ohtomo,[5,6] Konosuke Morimoto,[3] Masayuki Ishida,[3] Taro Kamigaki,[7] Hitoshi Oshitani,[7] Masahiro Hashizume,[8] Wataru Endo,[1] Koichi Hagiwara,[2] Koya Ariyoshi,[3] Shoji Okinaga[1,9]

► Additional material is published online only. To view please visit the journal online (http://dx.doi.org/10.1136/thoraxjnl-2012-202658).

[1]Kesennuma City Hospital, Kesennuma, Japan
[2]Department of Respiratory Medicine, Saitama Medical University, Saitama, Japan
[3]Department of Clinical Medicine, Institute of Tropical Medicine, Nagasaki University, Nagasaki, Japan
[4]Wayne State University, Detroit, Michigan, USA
[5]Ohtomo Hospital, Kesennuma, Japan
[6]Kesennuma City Medical Association, Kesennuma, Japan
[7]Department of Virology, Tohoku University Graduate School of Medicine, Sendai, Miyagi, Japan
[8]Department of Paediatric Infectious Diseases, Institute of Tropical Medicine, Nagasaki University, Nagasaki, Japan
[9]Institute of Development, Aging and Cancer, Tohoku University, Sendai, Miyagi, Japan

Correspondence to
Dr Motoi Suzuki, Department of Clinical Medicine, Institute of Tropical Medicine, Nagasaki University, Sakamoto 1-12-4, Nagasaki 852-8523, Japan; mosuzuki@nagasaki-u.ac.jp

Received 30 August 2012
Revised 25 January 2013
Accepted 29 January 2013
Published Online First 19 February 2013

To cite: Daito H, Suzuki M, Shiihara J, *et al*. *Thorax* 2013;**68**:544–550.

ABSTRACT

Background On 11 March 2011, the Tohoku earthquake and tsunami struck off the coast of northeastern Japan. Within 3 weeks, an increased number of pneumonia admissions and deaths occurred in local hospitals.

Methods A multicentre survey was conducted at three hospitals in Kesennuma City (population 74 000), northern Miyagi Prefecture. All adults aged ≥18 years hospitalised between March 2010 and June 2011 with community-acquired pneumonia were identified using hospital databases and medical records. Segmented regression analyses were used to quantify changes in the incidence of pneumonia.

Results A total of 550 pneumonia hospitalisations were identified, including 325 during the pre-disaster period and 225 cases during the post-disaster period. The majority (90%) of the post-disaster pneumonia patients were aged ≥65 years, and only eight cases (3.6%) were associated with near-drowning in the tsunami waters. The clinical pattern and causative pathogens were almost identical among the pre-disaster and post-disaster pneumonia patients. A marked increase in the incidence of pneumonia was observed during the 3-month period following the disaster; the weekly incidence rates of pneumonia hospitalisations and pneumonia-associated deaths increased by 5.7 times (95% CI 3.9 to 8.4) and 8.9 times (95% CI 4.4 to 17.8), respectively. The increases were largest among residents in nursing homes followed by those in evacuation shelters.

Conclusions A substantial increase in the pneumonia burden was observed among adults after the Tohoku earthquake and tsunami. Although the exact cause remains unresolved, multiple factors including population aging and stressful living conditions likely contributed to this pneumonia outbreak.

Key messages

What is the key question?

- Did the pneumonia incidence increase among the adult population after the Tohoku earthquake/tsunami, what were the characteristics of the disaster-associated pneumonia?

What is the bottom line?

- Our survey in a well defined population of northern Miyagi Prefecture revealed that a marked increase in the incidence of pneumonia hospitalisations and pneumonia-associated deaths was observed during the 3-month period following the disaster, the vast majority of the victims were older people, only 3.6% were associated with near-drowning in the tsunami waters, and the clinical and microbiological characteristics of the post-disaster patients were similar to those of the pre-disaster patients.

Why read on?

- Because this disaster affected a notably aging population with the highest baseline pneumonia incidence rate, the disaster caused a drastic increase in the number of admissions and placed a heavy burden on local hospitals. In addition to using the pneumococcal vaccine for disaster-affected populations, the provision of optimal living conditions, medical check-ups and oral hygiene care must be a priority for older people after natural disasters.

INTRODUCTION

On 11 March 2011, a magnitude 9.0 earthquake struck off the northeastern coast of Japan. Within an hour of the earthquake, devastating tsunamis swept over the east coast of the Tohoku Region, resulting in approximately 20 000 deaths and catastrophic damage to the local infrastructure and environment.[1 2] As a result of the extensive destruction of homes, more than 400 000 displaced people were moved to emergency evacuation shelters that were not supplied with electricity, gas, water or food, despite sub-freezing winter temperatures.[3 4]

Previous studies showed that acute respiratory infections were frequently observed among people displaced by the 2001 earthquake in El Salvador,[5] among those affected by the 2003 Bam earthquake

in Iran[6] and among people in Aceh Province affected by the 2004 Indian Ocean earthquake and tsunami.[7] Furthermore, severe pneumonia associated with the aspiration of seawater, known as 'tsunami lung', was reported in areas affected by the Indian Ocean tsunami.[8–10] However, these studies were conducted in resource-limited settings without reliable baseline data and lacked a standardised case definition. The impact of natural disasters, including tsunamis, on the risk of pneumonia remains largely unknown.

Within 3 weeks of the earthquake and tsunami on 11 March, a rapid increase in pneumonia hospitalisations and related deaths in northern Miyagi Prefecture was reported by mass media outlets.[11] We undertook an investigation to elucidate the impact of the Tohoku earthquake/tsunami on the incidence of pneumonia-related hospitalisations and mortality among adults aged ≥18 years in Kesennuma. We also sought to describe the clinical characteristics of disaster-related pneumonia and investigate the potential causes of increased rates of pneumonia in the affected population.

METHODS

Setting

Kesennuma is located on the northeastern coast of Miyagi Prefecture (figure 1). The city has a long, saw-toothed coastline with narrow, flat land facing the Pacific Ocean. The total population in February 2011 was 74 257 (source: Department of

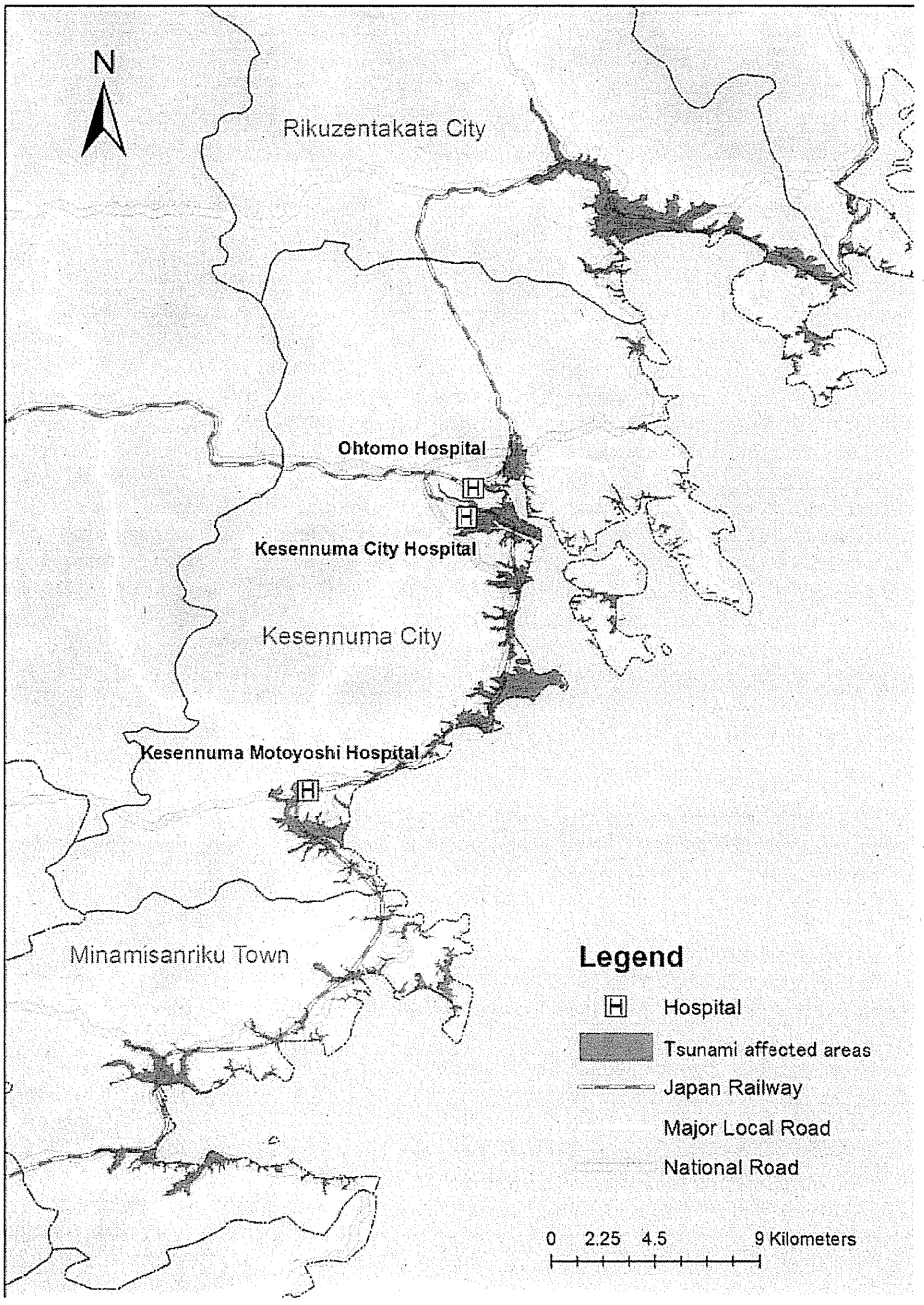

Figure 1 Area affected by the Tohoku earthquake and tsunami, Kesennuma City, Miyagi Prefecture. The disaster area data were obtained from the overview map of tsunami-affected areas released by the Geospatial Information Authority of Japan (http://www.gsi.go.jp/BOUSAI/h23_tohoku.html).

Vital Statistics, Kesennuma City). The city inhabitants included a substantial number of older adults: 30.2% (n=22 421) were aged ≥65 years and 8.9% (n=6618) were aged ≥80 years. These percentages were higher than the national averages (23% and 6.4%, respectively). At the time of the disaster, no national programme for the administration of the 23 valent polysaccharide pneumococcal vaccine (PPV23) existed in Japan, and its coverage among Kesennuma residents aged ≥65 years was <5%.

At 14 : 46 local time on 11 March 2011, the earthquake shook Kesennuma. The first large tsunami wave hit Kesennuma within a half hour of the earthquake, resulting in the deaths of 1032 residents; an additional 324 residents were listed as missing. The majority (>90%) of the victims died from drowning.[2]

The tsunamis devastated buildings, cars, ships and all other structures. Major oil tanks in the port were damaged and leaked petroleum, leading to massive conflagrations in the city. The main road was demolished to the north and the south, and the city was isolated (figure 1). In the aftermath, residents fled to evacuation shelters, including schools and public halls, to relatives' houses located on higher ground. The number of evacuees reached a peak on 17 March 2011 (20 105 individuals at 99 sites), while many other residents remained in their partially damaged houses.

In early April 2011, a considerable increase in pneumonia hospitalisations was reported from hospitals in northern Miyagi Prefecture. Media outlets reported that the outbreak may have been related to exposure to dried oil mist (ie, oil leaked from damaged storage tanks) or contaminated tsunami water.

Study design

In response to this outbreak, the Kesennuma City Hospital (KCH), the Kesennuma City Medical Association and Nagasaki University established an investigation team and initiated a multicentre survey on 12 May. The team identified three hospitals in Kesennuma that were providing inpatient care for patients with pneumonia before the disaster (KCH, 451 beds; Kesennuma Motoyoshi Hospital (KMH), 38 beds; and Ohtomo Hospital (OH), 78 beds). The team also identified an orthopaedic hospital and some clinics that had a small number of pneumonia admissions before the disaster (approximately 10 cases per year in total); however, their buildings were completely demolished, and their patients' records were unavailable. Therefore, we did not include those cases.

Case ascertainment

For the study period (defined as 1 March 2010 to 30 June 2011), all patients who were hospitalised with a diagnosis of pneumonia were enumerated from existing hospitalisation databases. Working as a panel, three qualified pulmonologists reviewed medical charts and chest radiographs (CXRs) in September 2011 using a standardised case definition based on the British Thoracic Society guidelines.[12] After reviewing the medical charts and CXRs, the panel's consensus CXR interpretations were recorded. Patients were classified as having any pneumonia if they showed pulmonary consolidation on CXR and any respiratory symptoms consistent with pneumonia. If a patient developed the disease 48 h after admission, the patient was classified as having hospital-acquired pneumonia and was excluded from further analysis. Repeated episodes of pneumonia in the same patient within a 2-week period were regarded as a single episode.

While inspecting hospitalisation records and CXRs, we realised that a considerable proportion of paper-based medical charts and CXRs in KMH were lost or damaged by the tsunami, and only discharge summaries were available. Therefore for analysis, the patients were classified into one of two pneumonia case categories: (1) *confirmed pneumonia* (full medical records were available and the presence of consolidation was confirmed by pulmonologists) and (2) *probable pneumonia* (detailed data and CXRs were not available, but the history described in the summary records was compatible with pneumonia). We defined pneumonia episodes as near-drowning related if patients were engulfed by the tsunami water on 11 March 2011, and their disease onset occurred within 4 weeks of the disaster.

Data collection

Demographic, clinical, radiographic, microbiological and evacuation site information was collected from the medical charts using a standardised abstraction form. The patients' addresses before the disaster were extracted from the hospital database and converted to geographical coordinates. Patients with pneumonia who died in any of the three study hospitals were categorised as fatal cases. The severity of pneumonia was assessed using the CURB65 scoring system.[13] Microbiological tests were routinely performed for clinically suspected cases throughout the study period at KCH, but they were not available at the other hospitals.

Data analysis

The demographic and clinical characteristics of the study patients were compared between the pre-disaster and post-disaster periods using χ^2 and Fisher's exact tests. The near-drowning-related cases were excluded from this comparison because the cause of disease was clear. The factors associated with death were assessed using Poisson regression models with robust SEs.[14] Pneumonia incidence and mortality rate calculations were limited to patients living in Kesennuma. The effects of the disaster, defined as a change in the weekly incidence of hospitalisations and associated deaths after the disaster (ie, the incidence rate ratios), were separately assessed using segmented generalised linear Poisson regression models allowing for overdispersion.[15] The regression models included terms for the disaster and time trends before and after the disaster. The change in the population size due to the disaster was taken into account using the offset function. Partial correlograms were used to assess serial autocorrelation of the residuals and, since there was no detectable autocorrelation, the data were modelled assuming independence.

Ethics

This study was approved by the Institutional Review Board of KCH.

RESULTS

Patients

Over the course of the study period (1 March 2010 to 30 June 2011), a total of 550 pneumonia cases were identified from hospital and facility records. According to the patients' disease onset, 225 confirmed cases and 100 probable cases occurred before 11 March and 225 confirmed cases occurred after 11 March (see online supplementary appendix figure 1). There was a sharp rise in the weekly number of pneumonia hospitalisations shortly after the disaster (figure 2A). A majority of the patients (95%) were city residents and their geographical distribution was similar across the study periods (see online supplementary appendix figure 2). When only city residents were included in the analysis, the highest incidence rate occurred during the first 2 weeks after the disaster, and the

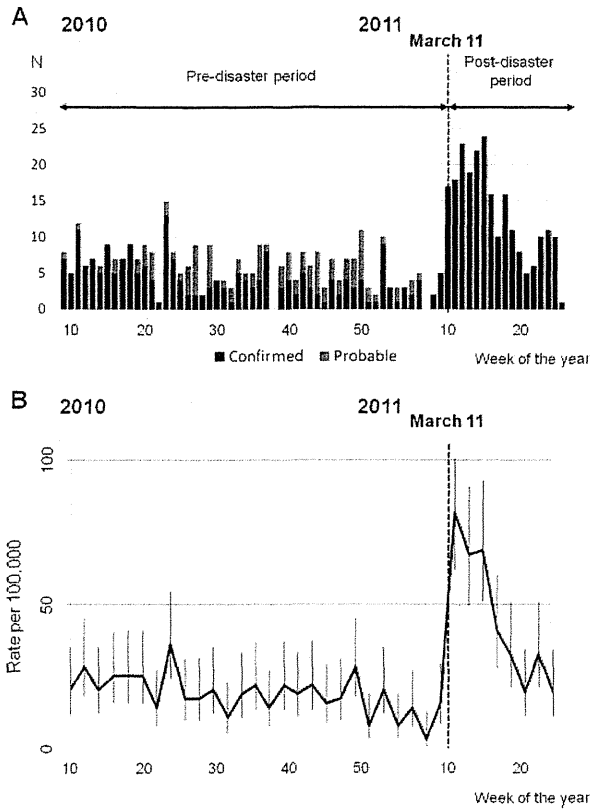

Figure 2 Trend of pneumonia hospitalisations in Kesennuma City, March 2010 to June 2011. (A) Weekly number of confirmed and probable cases according to the date of onset. (B) Biweekly incidence rates (per 100 000 people) calculated according to the date of onset. Cases were limited to the residents of Kesennuma City. The vertical lines indicate 95% CI.

incidence declined to the baseline level by mid-June 2011 (figure 2B).

To understand changes in the incidence of pneumonia, we compared the periods before (1 March 2010–10 March 2011) and after (11 March–30 June 2011) the disaster (table 1). The demographic and clinical pictures of disaster-related pneumonia were similar to those of pre-disaster cases, except that a substantial proportion (27.7%) of post-disaster patients were living in evacuation shelters. Nearly 90% of patients were older adults aged ≥65 years. The patients who were identified from evacuation shelters were younger (average age 76.7 years vs 80 years, p=0.047), less likely to have underlying medical conditions (45% vs 59.9%, p=0.049) and less likely to have fatal pneumonia (10% vs 29.3%, p=0.003) than patients with pneumonia identified from residences and nursing homes.

The patients identified from nursing homes were predominantly women, older and more likely to have had underlying conditions than were patients from homes and evacuation shelters. The proportion of patients with severe pneumonia with CURB65 ≥3 was high among patients from nursing homes, and those patients were more likely to die in the post-disaster period than in the pre-disaster period.

Incidence rates

During the three and a half months following 11 March, the weekly incidence of pneumonia hospitalisations increased by 5.7 times (95% CI 3.9 to 8.4) from the baseline level (table 2). The age group specific ratios were similar across all generations, whereas the absolute increase in the incidence was substantially greater among older people, especially those aged ≥80 years (the rate difference, 156.3 (95% CI 90.8 to 221.9) per 100 000 per population-week). The admission rate ratio was highest among nursing home residents followed by the residents of evacuation shelters. For pneumonia-related deaths, the rate increased by 8.9 times (95% CI 4.4 to 17.8) from the baseline level, and the mortality rate ratio was highest among nursing home residents.

Pneumonia aetiologies

Streptococcus pneumoniae, *Haemophilus influenzae* and *Klebsiella pneumoniae* were the leading causative pathogens identified in pre-disaster and post-disaster pneumonia cases. The positivity of *H influenzae* increased by fourfold after 11 March, especially among patients from evacuation shelters. *Staphylococcus aureus* was also found in patients throughout the study period, but its causative role was unclear (see online supplementary appendix table 1). None of the patients in this study were reported to have had positive rapid tests for influenza (the percentages tested before and after the disaster were 11.4% and 17.9%, respectively) or *Legionella pneumophila* serogroup 1 (28.4% and 35.5%, respectively).

Risk factors for death

Both before and after 11 March, a higher CURB65 score was significantly associated with an increased risk of death; the mortality also increased by age group, but the statistical evidence of this increase was weak. After the disaster, male gender and pre-hospital antibiotics use were associated with a higher risk of death after adjusting for other factors, and staying at an evacuation shelter was associated with a lower risk of death, although the significance was only marginal after adjustment. However, their effects on death were similar to the baseline figures (see online supplementary appendix table 2).

Near-drowning-related pneumonia

A history of exposure to tsunami water on 11 March was recorded in 10 patients. Among them, eight (3.6% of the disaster-related cases) were near-drowning-related pneumonia; seven were women, three were inside a car when engulfed by the tsunami, and one died from the disease. The median age was younger than that of other disaster-related pneumonia patients (62 years vs 79 years, p<0.001).

DISCUSSION

In this report, we documented a substantial increase in the rate of pneumonia-related hospital admissions and deaths in Kesennuma among adults of all age groups soon after the Tohoku earthquake and tsunami. The clinical and microbiological characteristics of the post-disaster patients were similar to those of the pre-disaster patients. The vast majority of the victims were older people. Because this disaster affected a notably aging population with the highest baseline pneumonia incidence rate, the disaster caused a drastic increase in the number of admissions and placed a heavy burden on local hospitals.

Although the causal mechanism was not fully established, our findings suggested that multiple factors have contributed to this outbreak. The largest increase in the pneumonia burden was observed in nursing home residents, the majority of which were older people with physical and mental limitations and needed assistance with daily activities. A sudden change in their living

Table 1 Characteristics of confirmed pneumonia cases by residence, before and after the 2011 Tohoku earthquake and tsunami, Kesennuma City, Miyagi, Japan

Characteristics	Pre-disaster period (1 March 2010–10 March 2011)†			Post-disaster period (11 March–30 June 2011)†				Pre-disaster vs post-disaster period p Value‡
	Residential category*			Residential category**				
	Total (n=225)	Home (n=193)	Nursing home (n=32)	Total (n=217)	Home (n=117)	Nursing home (n=40)	Evacuation shelter (n=60)	
Female sex (%)	98 (43.6)	77 (39.9)	21 (65.6)	93 (42.9)	46 (39.3)	26 (65)	21 (35)	0.882
Age category (%)								
18–49 years	13 (5.8)	12 (6.2)	1 (3.1)	4 (1.8)	3 (2.6)	0 (0)	1 (1.7)	0.161§
50–64 years	21 (9.3)	20 (10.4)	1 (3.1)	18 (8.3)	10 (8.6)	3 (7.5)	5 (8.3)	
65–79 years	61 (27.1)	56 (29)	5 (15.6)	67 (30.9)	32 (27.4)	6 (15)	29 (48.3)	
≥80 years	130 (57.8)	105 (54.4)	25 (78.1)	128 (59)	72 (61.5)	31 (77.5)	25 (41.7)	
Duration of symptoms before admission (%)								
≤2 days	109 (48.4)	91 (47.2)	18 (56.3)	114 (52.5)	59 (50.4)	25 (62.5)	30 (50)	0.434
3 days or more	109 (48.4)	96 (49.7)	13 (40.6)	98 (45.2)	54 (46.2)	14 (35)	30 (50)	
Antibiotics prescribed before admission (%)	32 (14.2)	23 (11.9)	9 (28.1)	29 (13.4)	7 (6)	10 (25)	12 (20)	0.794
With underlying conditions (%)	129 (57.3)	107 (55.4)	22 (68.7)	121 (55.8)	64 (54.7)	30 (75)	27 (45)	0.739
CURB65 score (%)								
3–5 (severe)	26 (11.6)	23 (11.9)	3 (9.4)	27 (12.4)	10 (8.6)	13 (32.5)	4 (6.7)	0.916
0–2 (less severe)	186 (82.7)	159 (82.4)	27 (84.4)	179 (82.5)	97 (82.9)	26 (65)	56 (93.3)	
Deceased (%)	39 (17.3)	31 (16.1)	8 (25)	52 (24)	28 (23.9)	18 (45)	6 (10)	0.085
Microbiological tests performed	145 (64.4)	129 (66.8)	16 (50)	139 (64.1)	74 (63.3)	22 (55)	43 (71.7)	0.932
Positive for *Streptococcus pneumoniae*¶	15 (6.7)	13 (6.7)	2 (6.3)	22 (10.1)	9 (7.7)	4 (10)	9 (15)	0.402
Positive for *Haemophilus influenzae*	3 (1.3)	3 (1.5)	0 (0)	14 (6.5)	7 (6)	0 (0)	7 (11.7)	0.013§
Positive for *Klebsiella pneumoniae*	8 (3.6)	6 (3.1)	2 (6.2)	11 (5.1)	5 (4.3)	4 (10)	2 (3.3)	0.698

*The characteristics differed by residential categories for gender (p=0.007) and pre-hospital antibiotic treatment (p=0.015).
†The pre-disaster and pos-disaster cases were categorised according to the date of onset. The near-drowning-related cases were excluded.
‡Characteristics were compared between the pre-disaster and post-disaster cases. χ^2 tests were performed unless otherwise indicated.
§Fisher's exact test.
¶Either a bacterial culture was isolated or a rapid urinary antigen test was positive.
**The characteristics differed by residential categories for gender (p=0.006), age group (p=0.012), pre-hospital antibiotic treatment (p=0.002), presence of underlying conditions (p=0.012), clinical severity (p<0.001) and fatality (p<0.001).

environment after the disaster, such as a lack of appropriate nutrition, the loss of regular medicines and a shortage of caregivers, must have worsened their conditions.[16] It should be noted that many caregivers were also victims who lost their families, friends and homes. This may have been reflected by the fact that the highest mortality rate among patients from nursing homes occurred in the early post-disaster period (results not shown). A high incidence was also observed in the residents of evacuation shelters. Crowding is a risk factor for *S pneumoniae* and *H influenzae* infection,[17 18] and we found that these pathogens, particularly *H influenzae*, were isolated more frequently in patients from evacuation shelters.

The increased incidence observed in all residential places suggests that other factors which were shared by all survivors have also played an important role. First, hypothermia is known to increase the risk of subsequent infections, including pneumonia.[19 20] On 11 March, it was snowing in northern Miyagi. All survivors were suddenly left without running water, gas, electricity or oil in freezing weather (−3 to −5°C at night; see online supplementary appendix figure 3). The majority of the evacuation shelters were not sufficiently equipped with heating and blankets immediately after the disaster. Second, people experience stress reactions after the disaster. Psychological stress weakens the immune system and may increase the risk of respiratory infections.[21 22] Third, the medical supply systems have drastically changed. Soon after the disaster, more than a hundred relief teams arrived in Kesennuma and initiated care for survivors; this change may have increased the chance of identifying patients with pneumonia.

The abovementioned reasons also explain the decline in pneumonia cases after May; the temperature increase, improvements in living conditions (water, gas and electricity had been fully restored by the end of May), recovery of medical supplies, and the decline in the number of evacuees reduced the risks of pneumonia. However, in our study, it was impossible to know what factors have truly contributed to this outbreak.

Pneumonia outbreaks after natural disasters have never been documented in the past. In 2005, Nishikiori and colleagues conducted a cross-sectional survey (n=3533 individuals) in Sri Lanka after the Indian Ocean tsunami,[23] and no deaths were reported between one week and two and a half months after the tsunami. The different findings in Sri Lanka may be explained by the difference in population structures. If we projected our age group-specific estimates onto a population in Sri Lanka, where the proportions of people aged ≥65 years and ≥80 years in 2004 were 7% and <0.5%, respectively, the overall impact on pneumonia admission and mortality would decrease by almost 80%. Therefore, it is plausible that the impact of